PHYSICAL REVIEW RESEARCH **4**, 023150 (2022)

Editors' Suggestion | Featured in Physics

Autoresonant excitation of space-time quasicrystals in plasma

Vadim R. Munirov,[1,*] Lazar Friedland,[2] and Jonathan S. Wurtele[1]

[1]*Department of Physics, University of California, Berkeley, California 94720, USA*

[2]*Hebrew University of Jerusalem, Jerusalem 91904, Israel*

(Received 7 January 2022; accepted 19 March 2022; published 25 May 2022)

We demonstrate theoretically and numerically that a warm fluid model of a plasma supports space-time quasicrystalline structures. These structures are highly nonlinear, two-phase, ion acoustic waves that are excited autoresonantly when the plasma is driven by two small amplitude chirped-frequency ponderomotive drives. The waves exhibit density excursions that substantially exceed the equilibrium plasma density. Remarkably, these extremely nonlinear waves persist even when the small amplitude drives are turned off. We derive the weakly nonlinear analytical theory by applying Whitham's averaged variational principle to the Lagrangian formulation of the fluid equations. The resulting system of coupled weakly nonlinear equations is shown to be in good agreement with fully nonlinear simulations of the warm fluid model. The analytical conditions and thresholds required for autoresonant excitation to occur are derived and compared to simulations. The weakly nonlinear theory guides and informs numerical study of how the two-phase quasicrystalline structure "melts" into a single phase traveling wave when one drive is below a threshold. These nonlinear structures may have applications to plasma photonics for extremely intense laser pulses, which are limited by the smallness of density perturbations of linear waves.

DOI: 10.1103/PhysRevResearch.4.023150

I. INTRODUCTION

Photonic crystals [1–4] built from conventional materials are routinely employed to focus, polarize, and manipulate light pulses. A periodic array of alternating dielectrics and plasmas called plasma photonic crystals (PPCs) has been the subject of much interest [5–19] owing to its optical properties. Besides crystals, Levine and Steinhardt [20] introduced quasicrystals—materials with properties that are ordered in space but do not possess an exact periodicity. Photonic quasicrystals have been studied extensively [21–28]. Moreover, crystals can be periodic not just in space but also in time. For example, the optical properties of photonic time crystals with a refractive index varying periodically in time have been investigated in Refs. [29–36]. The optical properties of the structures possessing periodicity both in space and time have been studied in Refs. [36–43].

Plasma photonic crystals have a major drawback where the plasmas are contained within solid material: They break down at high field intensity and are, therefore, incapable of controlling the laser pulses that are essential for many high energy density science applications. Purely plasma based structures, on the other hand, can withstand high intensity pulses. Many concepts for plasma-based optical elements have been proposed and built [44]. Plasma channels [45] routinely focus lasers for particle acceleration experiments. Over two decades ago, it was realized that resonant interactions [46] could be used for compression of intense pulses (replacing large compressor gratings). Plasma mirrors [47–50] are routinely used [51,52] at the National Ignition Facility (NIF) to improve performance in inertial fusion experiments. Laser-sculpted plasma grating structures [53,54] as well as polarization control using plasma structures [55–58] have been investigated. A significant challenge of plasma gratings is that their efficacy depends on the maximum variation in the index of refraction that can be achieved at the required spatial scale. Plasma density is well below critical density, and the density modulation should be as large as possible. This naturally leads to an exploration of nonlinear waves.

In this paper, we propose formation and control of space-time quasicrystalline structures in plasma through excitation of strongly nonlinear large amplitude multiphase ion acoustic waves that modulate plasma density in the desired way. It is known that a linear standing wave of the form $U(x,t) \propto \cos(kx)\cos(\omega t)$, which is periodic in both time and space, is formed by superposing two linear traveling waves of the same frequency ω, but propagating in the opposite direction. Nonlinearity of the media in some cases allows a generalization of linear standing waves to a waveform $U(x,t) = F(kx - \omega t, kx + \omega t)$, where F is a 2π-periodic nonlinear function of two phase variables and is also periodic in time and space. Recently, it was demonstrated that such nonlinear structures could be formed in plasma in the form of electron plasma [59] and ion acoustic [60] waves. It is also known that even more complex multiphase constructs of the form $U(x,t) = F(\theta_1, \theta_2, \ldots, \theta_N)$, where each phase is $\theta_i = k_i x - \omega_i t$, exist in other physical systems described by integrable nonlinear wave equations, such as the Korteweg-de Vries (KdV), nonlinear

*vmunirov@berkeley.edu

Schrödinger (NLS), and sine-Gordon (SG) equations [61]. Generally, multiphase functions F are very nontrivial and can be described by a complex analysis based on the inverse scattering transform (see, for example, Ref. [62] for the KdV case). The multiphase waves are 2π periodic in each of the phase variables, but if at least two of k_i or ω_i are not commensurate, function F is not exactly periodic in time and/or space and, thus, comprise a family of nontrivial space-time quasicrystals. But how can one excite such a multiphase wave in a given physical system? Because of the complexity of the waveform, a direct realization of a multiphase wave requires setting up precise initial conditions, making it an impractical, if not impossible, strategy for experiments even in the case of just two phases θ_1, θ_2. A possible way to circumvent the experimental difficulty of setting up the precise initial conditions is exploiting phase locking with small amplitude chirped-frequency traveling waves. In the past this approach was used in exciting multiphase solutions for integrable systems: KdV [63], NLS [64], SG [65], and the periodic Toda lattice [66]. The autoresonant excitation was also demonstrated for single phase large amplitude ion acoustic waves [67,68]. This suggests that perhaps the autoresonance could be used in a more general way to excite multiphase solutions for ion acoustic waves.

Here, we demonstrate, using a warm fluid plasma model, that a two-phase, strongly nonlinear ion acoustic wave can be generated and controlled. The wave is created by starting from zero and autoresonantly driving the system with two small amplitude chirped-frequency ponderomotive traveling waves. We show that slow passage of the driving waves through resonances in the plasma results in the continuing autoresonant (phase locked with both drives) excitation of the wave. The system sustains this double autoresonance as the driving frequencies vary in time by increasing the amplitude of the excited waveform, creating an extremely large amplitude space-time quasicrystal in plasma. This result is surprising and suggests some degree of integrability in the problem. We conjecture that this integrability is related to the fact that in the limit of small amplitude, ion acoustic waves are reduced to the KdV-type equation [69]. Since there exist many continuous physical systems approximated by the KdV, NLS, and SG equations, we expect that autoresonant space-time quasicrystals can be formed similarly in all these systems.

The paper is organized as follows. In Sec. II, we formulate the problem within a warm fluid plasma model and present a fully nonlinear numerical solution. In Sec. III, by using the Lagrangian formulation of the fluid equations and applying Whitham's averaged variational principle [70], we derive an analytical weakly nonlinear theory and demonstrate that it agrees well with the fully nonlinear simulations. In Sec. IV, we use our weakly nonlinear theory to study how to choose the parameters required to excite a two-phase autoresonant solution as well as discuss its threshold nature. Finally, in Sec. V, we summarize and discuss our results.

II. FORMULATION OF THE PROBLEM AND THE NUMERICAL RESULTS

We start with a warm fluid model of ion acoustic waves in plasma described by the following system of continuity, momentum, and Poisson's equations:

$$n_t + (nu)_x = 0, \tag{1}$$

$$u_t + uu_x = -\varphi_x - \Delta^2 nn_x, \tag{2}$$

$$\varphi_{xx} = e^{\varphi+\varphi_d} - n. \tag{3}$$

Here n is the ion density, u is the ion fluid velocity, $\Delta^2 = 3u_{th}^2$, where u_{th} is the ion thermal velocity, φ is the electric potential, and φ_d is the driving potential. All variables and parameters are dimensionless, such that the time is measured in terms of the inverse ion plasma frequency $\omega_{pi}^{-1} = \sqrt{m_i/m_e}\omega_p^{-1}$, the distance in terms of the Debye length $\lambda_D = u_e/\omega_p$, and, consequently, the velocities are measured in terms of the modified electron thermal velocity $\sqrt{m_e/m_i}u_e$. The plasma density and the electric potential are normalized with respect to the unperturbed plasma density and k_BT_e/e, respectively. The driving potential consists of two small amplitude (ε_1, ε_2) traveling waves and has the following form:

$$\varphi_d = \varepsilon_1 \cos(\theta_{d,1}) + \varepsilon_2 \cos(\theta_{d,2}), \tag{4}$$

where the traveling wave drives have driving phases $\theta_{d,i} = k_i x - \int \omega_{d,i}(t)dt$ with slowly varying driving frequencies $\omega_{d,i}(t) = -d\theta_{d,i}/dt$ $(i = 1, 2)$.

We can solve the system of the nonlinear equations (1)–(3) numerically using the water bag model method similar to the procedure described in Refs. [60,68].

To be specific, let us consider two driving counter propagating traveling waves with $k_1 = -0.5$ and $k_2 = 1$. We use linearly chirped driving frequencies for $t \leqslant 0$ and arctan drive for $t > 0$ $(i = 1, 2)$:

$$\omega_{d,i} = \begin{cases} \omega_{a,i} + \alpha_i t, & t \leqslant 0, \\ \omega_{a,i} + \alpha_i T_i \arctan\left(\frac{t}{T_i}\right), & t > 0. \end{cases} \tag{5}$$

Here, $\omega_{a,i}(k_i)$ $(i = 1, 2)$ are the frequencies given by the linear ion acoustic wave dispersion relation:

$$\omega_{a,i}(k_i) = |k_i|\sqrt{\frac{1}{1+k_i^2} + \Delta^2}, \tag{6}$$

and we use equal chirp rates $\alpha_1 = \alpha_2 = 2.5 \times 10^{-5}$ for $t \leqslant 0$ and $T_i = 2\Delta\omega_i/\pi\alpha_i$ $(i = 1, 2)$, $\Delta\omega_1 = \Delta\omega_2 = 0.07$ for $t > 0$. We also slowly build up the driving amplitudes as $\varepsilon_i = \bar{\varepsilon}_i[0.5 + \arctan(t/T_i)/\pi]$, $\bar{\varepsilon}_i = 16\alpha_i^{3/4}$ $(i = 1, 2)$ to have a smoother entrance into the autoresonant regime. The ion thermal velocity is chosen as $u_{th} = 0.003$.

The results of the numerical simulations are presented in Fig. 1. Figure 1(a) shows a colormap of the electron density $n_e(x, \tau)$ approximated by $e^{\varphi(x,\tau)}$ as a function of x and τ, where we introduced a slow time variable $\tau = \sqrt{\alpha_1}t$. We can clearly see in Fig. 1(a) a crystal-like quasiperiodic spatiotemporal structure representing a large amplitude ($\delta n_e/n_e \sim 1$) two-phase strongly nonlinear ion acoustic wave excited by the two driving counter propagating traveling waves. Figures 1(b) and 1(c) show a colormap of $n_e(x, \tau) \approx e^{\varphi(x,\tau)}$ but when driven by just one of the driving components with $k_1 = -0.5$ and $k_2 = 1$, respectively. We can see that an excitation of a

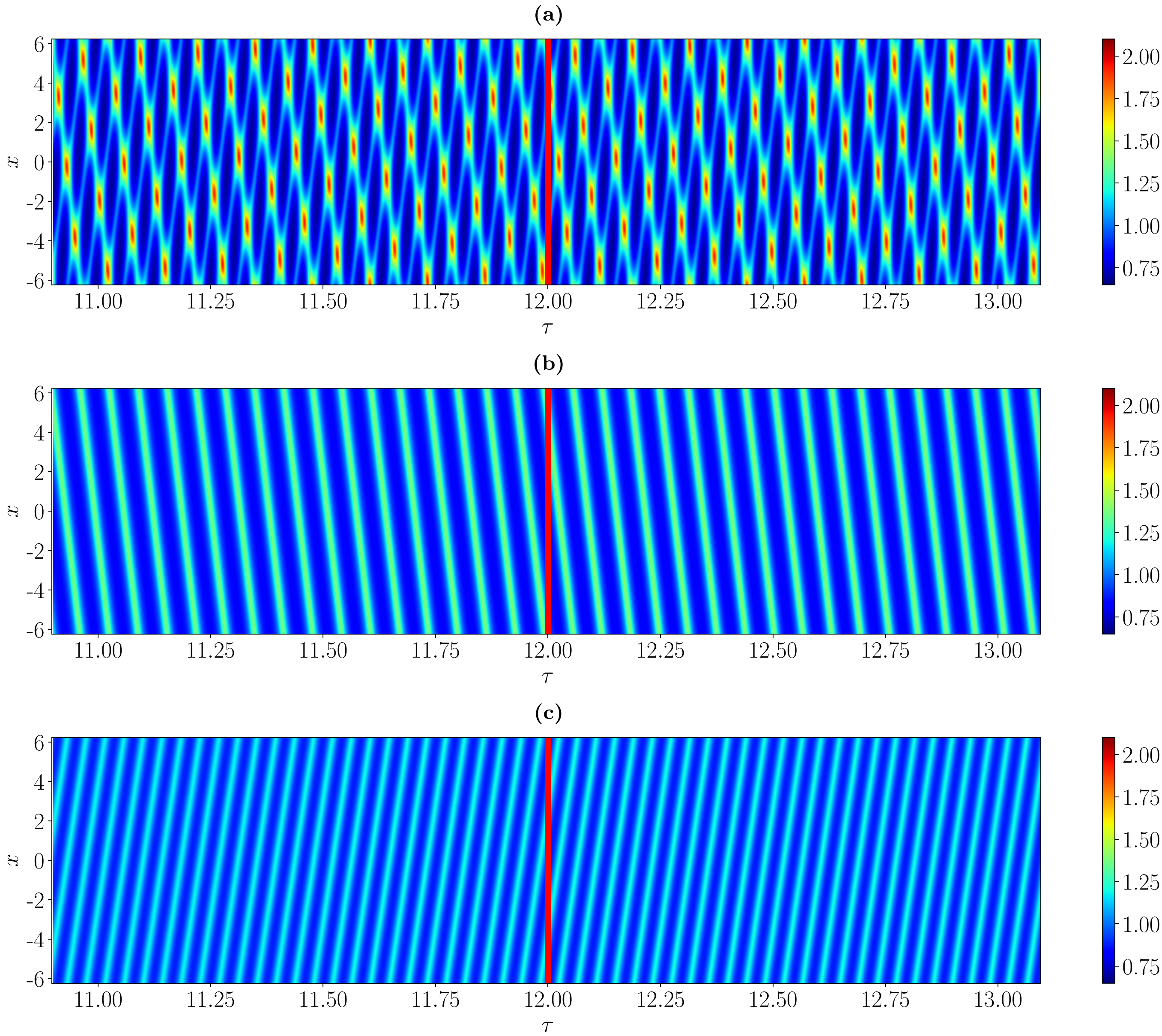

FIG. 1. The colormap of the electron density $n_e(x, \tau)$ as a function of slow time $\tau = \sqrt{\alpha_1}t$ and coordinate x. (a) Two-phase autoresonant ion acoustic wave excited by two driving counter propagating traveling waves with $k_1 = -0.5$ and $k_2 = 1$ obtained by solving the fully nonlinear equations (1)–(3). (b) Autoresonant single phase ion acoustic wave driven by the first driving component in (a) with $k_1 = -0.5$. (c) Autoresonant single phase ion acoustic wave driven by the second driving component in (a) with $k_2 = 1$. The red-vertical line indicates the termination of the drive at $\tau = 12$.

single phase large amplitude ion acoustic wave creates traveling wave-type spatiotemporal photonic plasma structures. In these single phase solutions the phases remain constant along the characteristic directions given by the phase velocity of the driving waves. The same two characteristic directions can also be seen in the two-phase wave solution in Fig. 1(a). We start our simulations at $\tau = -7$ and stop the driving at $\tau = 12$ (which is indicated by the red vertical line in Fig. 1. At $\tau = 0$ both driving waves pass the linear resonances and then the system enters the autoresonant regime and its excitation amplitude increases to preserve the resonances with the drives. This can be seen in Fig. 2, which shows the maximum value over x of the ion fluid velocity $u(x, \tau)$ versus slow time $\tau = \sqrt{\alpha_1}t$. Note that the crystal-like structure is preserved in time after we turn off the drive at $\tau = 12$, suggesting formation of some fundamental mode of the system.

The limiting factor as to what amplitudes we can excite the ion acoustic waves is determined by the kinetic wave breaking [60,68,71,72]. For the cold plasma this occurs when the ion fluid velocity exceeds the absolute value of the phase velocity of at least one of the driving waves. As we can see in Fig. 2, the maximum amplitude of the ion fluid velocity u stays below the absolute value of the phase velocities of the driving waves; we thereby avoid the wave-breaking limit for the parameters chosen in our example.

In the next section, we are going to cast the problem into the Lagrangian form and develop an adiabatic, weakly nonlinear theory using Whitham's averaged variational principle

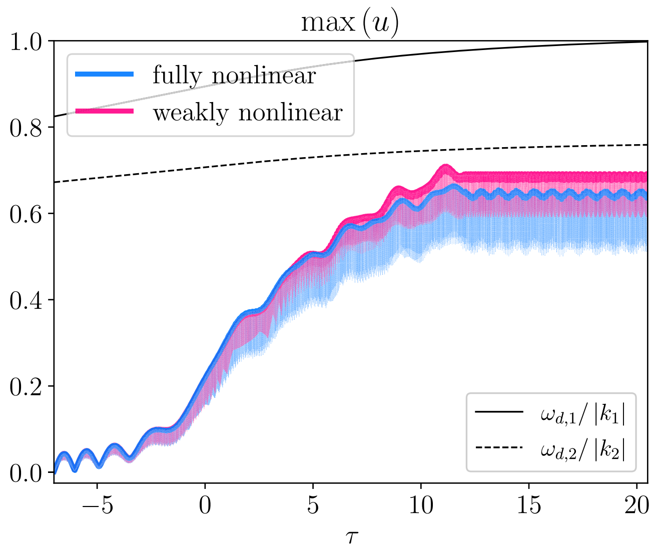

FIG. 2. The maximum (over x) of the ion fluid velocity $u(x,\tau)$ vs slow time $\tau = \sqrt{\alpha_1}t$ for a two-phase autoresonant ion acoustic wave excited by two driving traveling waves with $k_1 = -0.5$ and $k_2 = 1$ obtained by solving the fully nonlinear equations (1)–(3) (denoted as "fully nonlinear", blue line) and the weakly nonlinear reduced dynamical equations (38)–(41) (denoted as "weakly nonlinear", pink line). The solid-black line represents the absolute value of the phase velocity $\omega_{d,1}(\tau)/|k_1|$ of the first driving wave and the dashed-black line represents the absolute value of the phase velocity of the second driving wave $\omega_{d,2}(\tau)/|k_2|$ vs τ. The parameters used in the simulations are the same as in Figs. 1(a), 3, and 4

[70]. These analytical results will allow us to understand how to control and choose parameters for the excitation of large amplitude multiphase ion acoustic waves.

III. THE LAGRANGIAN FORMULATION AND WHITHAM'S VARIATIONAL PRINCIPLE

For convenience, let us introduce two new potentials ψ and σ via $u = \psi_x$, $n = 1 + \sigma_x$. The system of the nonlinear equations (1)–(3) in terms of the new variables is then

$$\sigma_{xt} + [(1+\sigma_x)\psi_x]_x = 0, \tag{7}$$

$$\psi_{xt} + \psi_x\psi_{xx} = -\varphi_x - \Delta^2(1+\sigma_x)\sigma_{xx}, \tag{8}$$

$$\varphi_{xx} \approx (1+\varphi_d)e^{\varphi} - \sigma_x - 1, \tag{9}$$

where we assumed that the drive is small: $e^{\varphi_d} \approx 1 + \varphi_d$.

Equations (7)–(9) can be derived from the Lagrangian variational principle $\delta(\int L dx dt) = 0$ with the corresponding Lagrangian density L given by

$$L = \frac{1}{2}\varphi_x^2 + V(\varphi) - \frac{1}{2}(\psi_t\sigma_x + \psi_x\sigma_t) - \left(\frac{1}{2}\psi_x^2 + \varphi\right)(1+\sigma_x) - \frac{\Delta^2}{2}\sigma_x^2\left(1 + \frac{1}{3}\sigma_x\right) + \varphi_d\varphi, \tag{10}$$

where $V(\varphi) = \varphi + \frac{1}{2}\varphi^2 + \frac{1}{6}\varphi^3 + \frac{1}{24}\varphi^4$.

The Lagrangian form of the problem together with the slow adiabatic synchronization (autoresonance) procedure we employ to excite multiphase waves suggest that it should be possible to use Whitham's averaged variational principle [70] to derive weakly nonlinear analytical results for our problem.

We proceed by writing the following ansatz describing the two-phase $[\theta_1 = k_1 x - \int \omega_1(t)dt,\ \theta_2 = k_2 x - \int \omega_2(t)dt]$ solutions for the potentials σ, ψ, φ:

$$\begin{aligned}\sigma &= \tilde{A}_{10}\sin(\theta_1) + \tilde{A}_{01}\sin(\theta_2)\\ &\quad + \tilde{A}_{11}\sin(\theta_1+\theta_2) + \tilde{A}_{1,-1}\sin(\theta_1-\theta_2)\\ &\quad + \tilde{A}_{20}\sin(2\theta_1) + \tilde{A}_{02}\sin(2\theta_2),\end{aligned} \tag{11}$$

$$\begin{aligned}\psi &= \tilde{B}_{10}\sin(\theta_1) + \tilde{B}_{01}\sin(\theta_2)\\ &\quad + \tilde{B}_{11}\sin(\theta_1+\theta_2) + \tilde{B}_{1,-1}\sin(\theta_1-\theta_2)\\ &\quad + \tilde{B}_{20}\sin(2\theta_1) + \tilde{B}_{02}\sin(2\theta_2),\end{aligned} \tag{12}$$

$$\begin{aligned}\varphi &= C_{00} + C_{10}\cos(\theta_1) + C_{01}\cos(\theta_2)\\ &\quad + C_{11}\cos(\theta_1+\theta_2) + C_{1,-1}\cos(\theta_1-\theta_2)\\ &\quad + C_{20}\cos(2\theta_1) + C_{02}\cos(2\theta_2).\end{aligned} \tag{13}$$

Here, we view the amplitudes $\tilde{A}_{10}, \tilde{A}_{01}, \tilde{B}_{10}, \tilde{B}_{01}, C_{10}, C_{01}$ as the first-order coefficients, while the amplitudes $\tilde{A}_{20}, \tilde{A}_{02}, \tilde{B}_{20}, \tilde{B}_{02}, C_{20}, C_{02}, \tilde{A}_{11}, \tilde{A}_{1,-1}, \tilde{B}_{11}, \tilde{B}_{1,-1}, C_{11}, C_{1,-1}$, and C_{00} as the second-order coefficients. It is also convenient to write the driving potential φ_d in the form with explicit phase mismatches $\Phi_i = \theta_i - \theta_{d,i}$ $(i = 1, 2)$ between phases of the solutions θ_1, θ_2 and the driving phases $\theta_{d,1}, \theta_{d,2}$:

$$\varphi_d = \varepsilon_1\cos(\theta_1 - \Phi_1) + \varepsilon_2\cos(\theta_2 - \Phi_2). \tag{14}$$

Furthermore, here and in the following it is assumed that the phases θ_1, θ_2 are varying rapidly, while all the coefficients in our ansatz and Φ_1, Φ_2 are slow functions of time.

In the linear case without phase mismatches we have the following solutions:

$$\sigma = \tilde{A}_{10}\sin(\theta_1) + \tilde{A}_{01}\sin(\theta_2), \tag{15}$$

$$\psi = \tilde{B}_{10}\sin(\theta_1) + \tilde{B}_{01}\sin(\theta_2), \tag{16}$$

$$\varphi = C_{10}\cos(\theta_1) + C_{01}\cos(\theta_2), \tag{17}$$

where the amplitudes C_{10} and C_{01} satisfy

$$C_{10}\left(\frac{k_1^2}{\omega_1^2 - \Delta^2 k_1^2} - 1 - k_1^2\right) = \varepsilon_1, \tag{18}$$

$$C_{01}\left(\frac{k_2^2}{\omega_2^2 - \Delta^2 k_2^2} - 1 - k_2^2\right) = \varepsilon_2, \tag{19}$$

and the amplitudes $\tilde{A}_{10}, \tilde{A}_{01}, \tilde{B}_{10}, \tilde{B}_{01}$ are expressed through C_{10} and C_{01} as follows:

$$\tilde{A}_{10} = \frac{k_1}{\omega_1^2 - \Delta^2 k_1^2}C_{10}, \tag{20}$$

$$\tilde{A}_{01} = \frac{k_2}{\omega_2^2 - \Delta^2 k_2^2}C_{01}, \tag{21}$$

$$\tilde{B}_{10} = \frac{\omega_1}{\omega_1^2 - \Delta^2 k_1^2}C_{10}, \tag{22}$$

$$\tilde{B}_{01} = \frac{\omega_2}{\omega_2^2 - \Delta^2 k_2^2}C_{01}. \tag{23}$$

The next crucial step is to find the averaged Lagrangian density over the rapidly varying phases θ_1, θ_2:

$$\bar{L} = \langle L(\theta_1, \theta_2, t)\rangle_{\theta_1,\theta_2} = \int L(\theta_1, \theta_2, t)\frac{d\theta_1}{2\pi}\frac{d\theta_2}{2\pi}, \qquad (24)$$

which will depend only on slow variables: the amplitudes of various harmonics and the phase mismatches.

After long but straightforward calculations one can obtain the average of Eq. (10) over the rapidly varying phases. This derivation of the averaged Lagrangian can be found in Appendix A.

Weakly nonlinear equations

Now, having obtained the averaged Lagrangian, we can derive the weakly nonlinear equations that describe the evolution of the wave amplitude by applying Whitham's variational procedure [70].

First, we take variations with respect to the phases:

$$\frac{d}{dt}\left(\frac{\partial \bar{L}}{\partial \dot{\theta}_1}\right) - \frac{\partial \bar{L}}{\partial \theta_1} = -\frac{d}{dt}\left(\frac{\partial \bar{L}}{\partial \omega_1}\right) - \frac{\partial \bar{L}}{\partial \Phi_1} = 0, \qquad (25)$$

$$\frac{d}{dt}\left(\frac{\partial \bar{L}}{\partial \dot{\theta}_2}\right) - \frac{\partial \bar{L}}{\partial \theta_2} = -\frac{d}{dt}\left(\frac{\partial \bar{L}}{\partial \omega_2}\right) - \frac{\partial \bar{L}}{\partial \Phi_2} = 0. \qquad (26)$$

Keeping the lowest significant order terms and using the linear relations (20)–(23), we get

$$\frac{d}{dt}\left[\frac{\omega_1 k_1^2}{\left(\omega_1^2 - \Delta^2 k_1^2\right)^2} C_{10}^2\right] = \varepsilon_1 C_{10} \sin(\Phi_1), \qquad (27)$$

$$\frac{d}{dt}\left[\frac{\omega_2 k_2^2}{\left(\omega_2^2 - \Delta^2 k_2^2\right)^2} C_{01}^2\right] = \varepsilon_2 C_{01} \sin(\Phi_2). \qquad (28)$$

Likewise, we can obtain from the variations with respect to the first-order amplitudes [see Eqs. (B42)–(B47) in Appendix B]:

$$\begin{aligned}\left(\frac{k_1^2}{\omega_1^2 - \Delta^2 k_1^2} - 1 - k_1^2\right)C_{10} &= C_{10}^2 P(k_1, \omega_1)C_{10} + C_{01}C_{10}Q(k_1, \omega_1; k_2, \omega_2)C_{01} \\ &\quad + \varepsilon_1 \cos(\Phi_1),\end{aligned} \qquad (29)$$

$$\begin{aligned}\left(\frac{k_2^2}{\omega_2^2 - \Delta^2 k_2^2} - 1 - k_2^2\right)C_{01} &= C_{01}^2 P(k_2, \omega_2)C_{01} + C_{01}C_{10}Q(k_1, \omega_1; k_2, \omega_2)C_{10} \\ &\quad + \varepsilon_2 \cos(\Phi_2),\end{aligned} \qquad (30)$$

where the functions $P(k_1, \omega_1)$ and $Q(k_1, \omega_1; k_2, \omega_2)$ are defined in Appendix C.

Expanding around the linear ion acoustic dispersion relation $\omega_i = \omega_{a,i} + \Delta\omega_i$ $(i = 1, 2)$, we get from Eqs. (29) and (30) the following expressions:

$$\begin{aligned}\Delta\omega_1 = &-\frac{\left(\omega_1^2 - \Delta^2 k_1^2\right)^2}{2\omega_1 k_1^2} P(k_1, \omega_1)C_{10}^2 \\ &- \frac{\left(\omega_1^2 - \Delta^2 k_1^2\right)^2}{2\omega_1 k_1^2} Q(k_1, \omega_1; k_2, \omega_2)C_{01}^2 \\ &- \frac{\left(\omega_1^2 - \Delta^2 k_1^2\right)^2}{2\omega_1 k_1^2}\frac{\varepsilon_1}{C_{10}}\cos(\Phi_1),\end{aligned} \qquad (31)$$

$$\begin{aligned}\Delta\omega_2 = &-\frac{\left(\omega_2^2 - \Delta^2 k_2^2\right)^2}{2\omega_2 k_2^2} P(k_2, \omega_2)C_{01}^2 \\ &- \frac{\left(\omega_2^2 - \Delta^2 k_2^2\right)^2}{2\omega_2 k_2^2} Q(k_1, \omega_1; k_2, \omega_2)C_{10}^2 \\ &- \frac{\left(\omega_2^2 - \Delta^2 k_2^2\right)^2}{2\omega_2 k_2^2}\frac{\varepsilon_2}{C_{01}}\cos(\Phi_2).\end{aligned} \qquad (32)$$

The above expressions (31) and (32) show that due to the nonlinear nature of the system, the waves acquire frequency shifts (the first two terms), which can be adjusted to the chirped driving frequencies continuously (see the last term), yielding control of the wave amplitudes.

Assuming linear driving frequency chirps $\omega_{d,i} = \omega_{a,i} + \alpha_i t$ $(i = 1, 2)$ and defining

$$I_1 = \frac{2\omega_1 k_1^2}{\left(\omega_1^2 - \Delta^2 k_1^2\right)^2} C_{10}^2, \quad I_2 = \frac{2\omega_2 k_2^2}{\left(\omega_2^2 - \Delta^2 k_2^2\right)^2} C_{01}^2, \qquad (33)$$

$$a = \frac{\left(\omega_1^2 - \Delta^2 k_1^2\right)^4}{4\omega_1^2 k_1^4} P(k_1, \omega_1), \qquad (34)$$

$$b = \frac{\left(\omega_1^2 - \Delta^2 k_1^2\right)^2}{2\omega_1 k_1^2}\frac{\left(\omega_2^2 - \Delta^2 k_2^2\right)^2}{2\omega_2 k_2^2} Q(k_1, \omega_1, k_2, \omega_2), \qquad (35)$$

$$c = \frac{\left(\omega_2^2 - \Delta^2 k_2^2\right)^4}{4\omega_2^2 k_2^4} P(k_2, \omega_2), \qquad (36)$$

$$\epsilon_1 = \frac{2\left(\omega_1^2 - \Delta^2 k_1^2\right)}{|k_1|}\varepsilon_1, \quad \epsilon_2 = \frac{2\left(\omega_2^2 - \Delta^2 k_2^2\right)}{|k_2|}\varepsilon_2, \qquad (37)$$

we can rewrite Eqs. (27), (28), (31), and (32) to obtain the following system of weakly nonlinear evolution equations:

$$\frac{dI_1}{dt} = \epsilon_1\sqrt{\frac{I_1}{2\omega_1}}\sin(\Phi_1), \qquad (38)$$

$$\frac{dI_2}{dt} = \epsilon_2\sqrt{\frac{I_2}{2\omega_2}}\sin(\Phi_2), \qquad (39)$$

$$\frac{d\Phi_1}{dt} = aI_1 + bI_2 + \alpha_1 t + \frac{\epsilon_1}{2\sqrt{2\omega_1 I_1}}\cos(\Phi_1), \qquad (40)$$

$$\frac{d\Phi_2}{dt} = bI_1 + cI_2 + \alpha_2 t + \frac{\epsilon_2}{2\sqrt{2\omega_2 I_2}}\cos(\Phi_2). \qquad (41)$$

Here, in principle, the linear frequency chirps $\alpha_i t$ $(i = 1, 2)$ can be replaced by any other functions of time as long as these functions are sufficiently slow. In fact, we use the arctan frequency chirp drive defined in Eq. (5) in our simulations.

The numerical solution of the weakly nonlinear system (38)–(41) is presented in Figs. 2–4. We use the drive and other parameters identical to those used in the numerical solution of the fully nonlinear system described in the previous section, which is presented in Figs. 1(a) and 2. As can be seen in Fig. 2 and by comparison between Figs. 1(a) and 3, the analytically derived weakly nonlinear system is indeed a good approximation of the fully nonlinear problem. We further observe in Fig. 2 the absence of the low frequency modulation in the weakly nonlinear solution after we stop driving at $\tau = 12$.

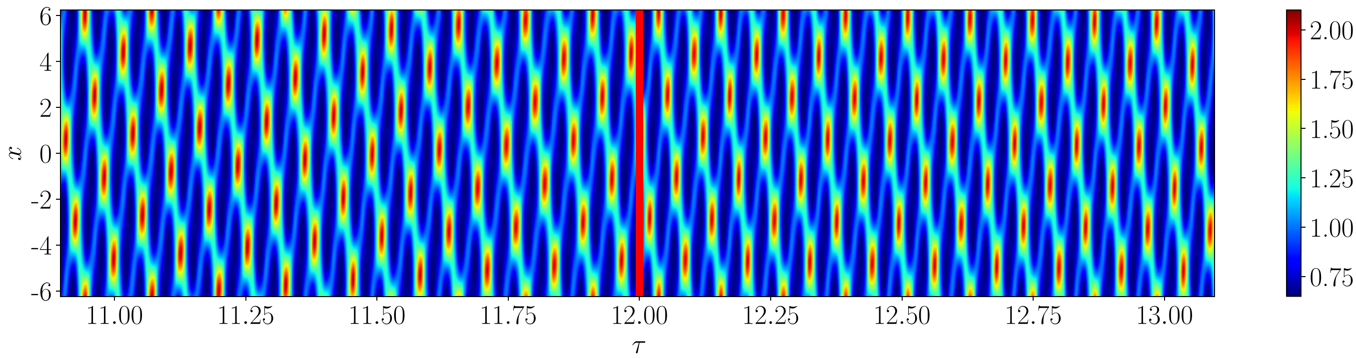

FIG. 3. The colormap of the electron density $n_e(x, \tau)$ as a function of slow time $\tau = \sqrt{\alpha_1}t$ and coordinate x for a two-phase autoresonant ion acoustic wave excited by two driving counter propagating traveling waves with $k_1 = -0.5$ and $k_2 = 1$ obtained by solving the weakly nonlinear reduced dynamical equations (38)–(41). The red-vertical line indicates the termination of the drive at $\tau = 12$. The parameters used in the simulation are the same as in Figs. 1(a), 2, and 4.

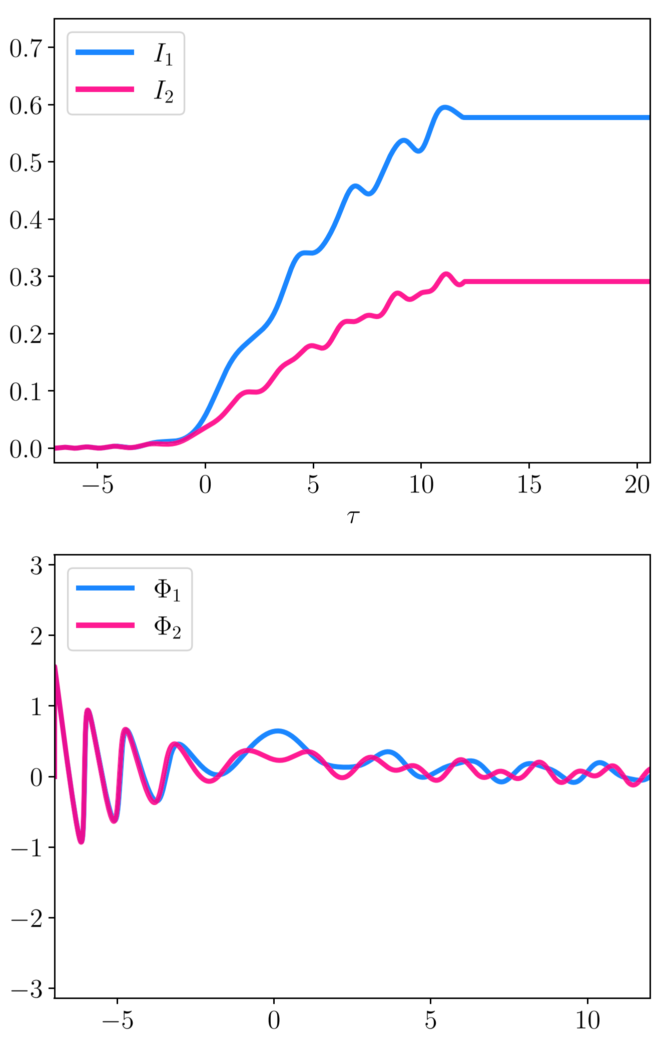

FIG. 4. The effective actions I_1, I_2 (top subplot) and the phase mismatches Φ_1, Φ_2 (bottom subplot) vs slow time $\tau = \sqrt{\alpha_1}t$ obtained by solving the weakly nonlinear reduced dynamical equations (38)–(41). The parameters used in the simulation are the same as in Figs. 1(a), 2, and 3.

The reason is that in this case $I_1, I_2 = \text{const}$, as evident from Eqs. (38)–(39), which implies that all the slowly evolving amplitudes are constant as well, while Eqs. (11)–(13) show that it is the slowly evolving amplitudes that are directly responsible for the low frequency modulation.

The nature of the autoresonant excitation and phase locking is demonstrated in Fig. 4, which shows the effective actions I_1, I_2 (top subplot) and the phase mismatches Φ_1, Φ_2 (bottom subplot) as functions of slow time $\tau = \sqrt{\alpha_1}t$. We can clearly see that as the system passes the linear resonance at $\tau = 0$, the phase mismatches are locked around zero, while the effective actions I_1, I_2 both enter the autoresonant regime and grow in amplitude. At $\tau = 12$ we turn off the drives and so the effective actions remain constant. In the absence of the drives, the phase mismatches are not meaningfully defined, therefore Φ_1, Φ_2 are shown in the figures only until $\tau = 12$.

We can explicitly test whether our assumption regarding the form of the ansatz used [see Eqs. (11)–(13)] is justified by performing the spectral analysis. Figure 5 shows the spectral distribution of the harmonics of the ion fluid velocity $u(x, \tau)$ in k space at two moments of time: $\tau = 3$ (pink line) and $\tau = 12$ (blue line), both in linear scale (top subplot) and in logarithmic scale (bottom subplot). We can see that the spectrum falls off dramatically with the increase in $|k|$; only a handful of harmonics have a noticeable weight and can be considered excited. At $\tau = 3$ the excited harmonics correspond to the ones used in the ansatz, so we see a very good agreement between the weakly nonlinear and the fully nonlinear solutions, as evident in Fig. 2. At $\tau = 12$ we can see that harmonics with $|k| = 2$ and $|k| = 2.5$, which are beyond the ones used in the ansatz, acquire some small but not non-negligible weights, so the agreement between the weakly nonlinear theory utilizing the ansatz given by Eqs. (11)–(13) and the fully nonlinear theory is not as good as at $\tau = 3$, though it is still decent. Thus, by checking the spectrum of the solutions, one can verify whether the ansatz is adequate for the parameters used in the simulations, and if necessary the ansatz can be extended to include more harmonics and more precise weakly analytical theory can be developed.

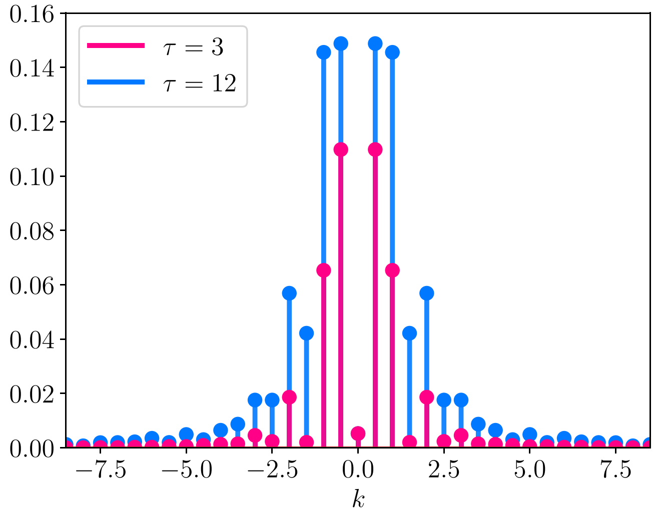

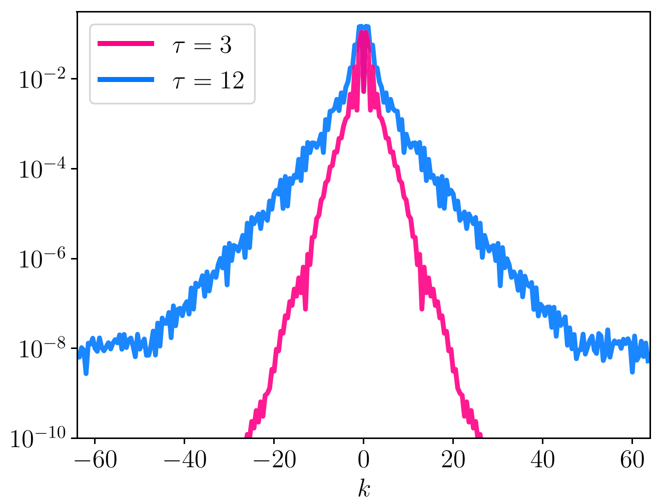

FIG. 5. The spectrum of the harmonics of the ion fluid velocity $u(x, \tau)$ in k space obtained by solving the fully nonlinear equations (1)–(3) at $\tau = 3$ (pink line) and $\tau = 12$ (blue line) in linear (top subplot) and logarithmic (bottom subplot) scales. The parameters used in the simulations are the same as in Figs. 1(a), 2, 3, and 4.

IV. THE CONDITIONS FOR DOUBLE AUTORESONANCE

Equations (38)–(41) have the same form as a weakly nonlinear system studied in Ref. [73]. Such a system is described by the following Hamiltonian for the effective action (I_1, I_2) and angle (Φ_1, Φ_2) variables:

$$H = \omega_1 I_1 + \omega_2 I_2 + \tfrac{1}{2} a I_1^2 + b I_1 I_2 + \tfrac{1}{2} c I_2^2 + f(I_1, I_2, \Phi_1, \Phi_2, t), \tag{42}$$

where

$$f(I_1, I_2, \Phi_1, \Phi_2, t) = \epsilon_1 \sqrt{\frac{I_1}{2\omega_1}} \cos(\Phi_1) + \epsilon_2 \sqrt{\frac{I_2}{2\omega_2}} \cos(\Phi_2). \tag{43}$$

As shown in Ref. [73], the possibility of double autoresonance is determined by the signs of $D = ac - b^2$ and $\alpha_1 \alpha_2$: for the double autoresonance to occur, they must have the same sign. From Eqs. (38)–(41), we see that in the case of the double autoresonance the asymptotic large t solutions for

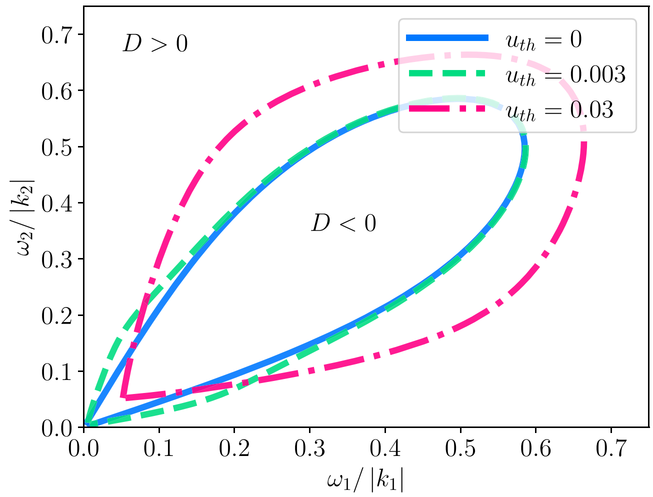

FIG. 6. The curves $D(k_1, k_2) = 0$ for three values of the ion thermal velocity: $u_{th} = 0$ (solid-blue line), $u_{th} = 0.003$ (dashed-green line), and $u_{th} = 0.03$ (dash-dotted-pink line), plotted in the $(\omega_1/|k_1|, \omega_2/|k_2|)$ plane assuming $k_1 k_2 > 0$. D is negative inside the curve $D = 0$ and positive outside the curve. For $k_1 k_2 < 0$, D is always positive. The double autoresonance is possible only in the regions where $D > 0$.

the actions are given by

$$\bar{I}_1 = \frac{b\alpha_2 - c\alpha_1}{D} t, \quad \bar{I}_2 = \frac{b\alpha_1 - a\alpha_2}{D} t. \tag{44}$$

Thus, in addition, for the double autoresonance to actually happen the asymptotic actions $\bar{I}_1$, $\bar{I}_2$ defined above must be positive.

There are two possible situations, depending on whether k_1 and k_2 have the same sign: (1) If $k_1 k_2 > 0$, we have $b < 0$, $a < 0$, $c < 0$. In this case D can have both positive and negative values. Figure 6 shows the lines for $D = 0$ in the plane formed by the absolute values of the phase velocities of the driving waves $(\omega_1/|k_1|, \omega_2/|k_2|)$ for different values of the ion thermal velocity u_{th}. We can see that the ion thermal velocity u_{th}, though not an extremely sensitive parameter, nevertheless determines the regions of positive and negative values of D. Thus the cold ion model should be used carefully and the thermal ion velocity should in general be taken into account. In the region where $D > 0$, for the double autoresonance to occur $\alpha_1 \alpha_2$ must be positive. In addition, for positive $\bar{I}_1$, $\bar{I}_2$ we must have $|b|/|a| < \alpha_2/\alpha_1 < |c|/|b|$. In contrast, if $D < 0$, we must have $\alpha_1 \alpha_2 < 0$. However, in this case it is impossible for both $\bar{I}_1$ and $\bar{I}_2$ to be positive at the same time. Thus, if $k_1 k_2 > 0$, the double autoresonance is possible only in the region where $D > 0$; in this region we also must have $\alpha_1 \alpha_2 > 0$ and $|b|/|a| < \alpha_2/\alpha_1 < |c|/|b|$. (2) The second possibility is $k_1 k_2 < 0$, then we have $b > 0$, $a < 0$, $c < 0$. In this case D is always positive, and, consequently, for double autoresonance we must have $\alpha_1 \alpha_2 > 0$. In addition, to have positive $\bar{I}_1$, $\bar{I}_2$ only the case when both α_1, α_2 are positive works. Thus, in the case where $k_1 k_2 < 0$, the double autoresonance is possible when $\alpha_1, \alpha_2 > 0$. We do not deal with the degenerate case of $k_1 = k_2$ in this paper.

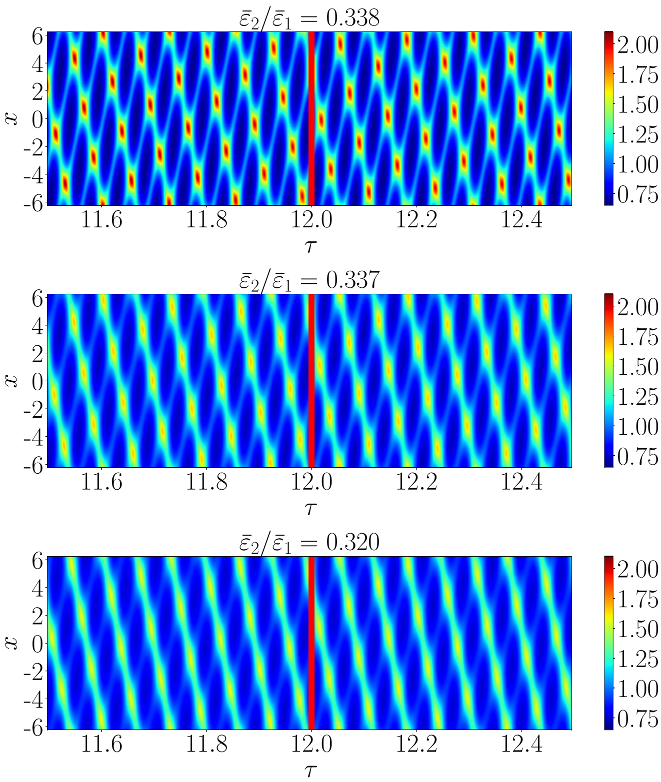

FIG. 7. Melting of a two-phase quasicrystal into a single phase quasicrystal around the threshold in the fully nonlinear model. The colormaps show the electron density $n_e(x, \tau)$ in the (x, τ) plane for a two-phase ion acoustic wave excited by two driving counter propagating traveling waves with $k_1 = -0.5$ and $k_2 = 1$ obtained by solving the fully nonlinear equations (1)–(3) for various values of $\bar{\varepsilon}_2$: just above the threshold ($\bar{\varepsilon}_2/\bar{\varepsilon}_1 = 0.338$, top subplot), just below the threshold ($\bar{\varepsilon}_2/\bar{\varepsilon}_1 = 0.337$, middle subplot), and below the threshold ($\bar{\varepsilon}_2/\bar{\varepsilon}_1 = 0.32$, bottom subplot). The parameters used in the simulations are otherwise the same as in Figs. 1(a), 2, and 3. The red-vertical line indicates the termination of the drive at $\tau = 12$.

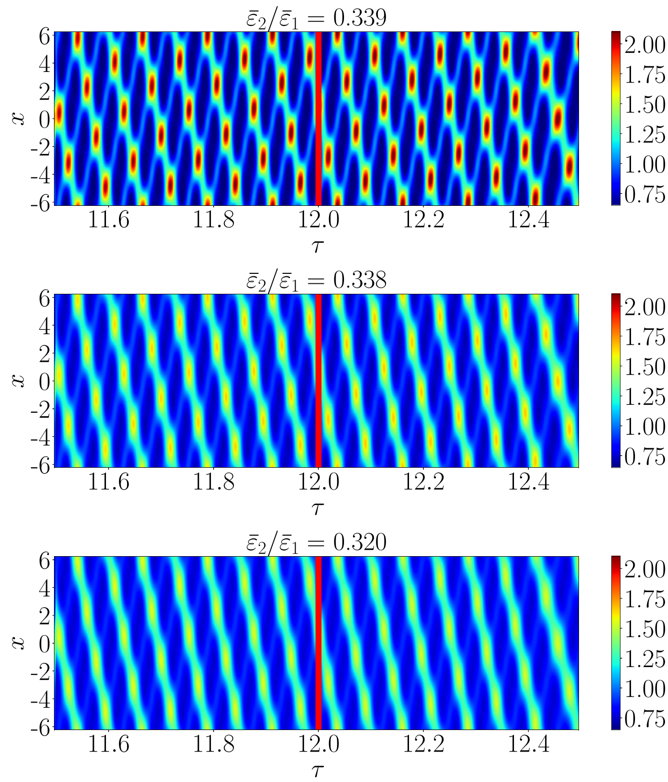

FIG. 8. Melting of a two-phase quasicrystal into a single phase quasicrystal around the threshold in the weakly nonlinear model. The colormaps show the electron density $n_e(x, \tau)$ in the (x, τ) plane for a two-phase ion acoustic wave excited by two driving counter propagating traveling waves with $k_1 = -0.5$ and $k_2 = 1$ obtained by solving the weakly nonlinear reduced dynamical equations (38)–(41) for various values of $\bar{\varepsilon}_2$: just above the threshold ($\bar{\varepsilon}_2/\bar{\varepsilon}_1 = 0.339$, top subplot), just below the threshold ($\bar{\varepsilon}_2/\bar{\varepsilon}_1 = 0.338$, middle subplot), and below the threshold ($\bar{\varepsilon}_2/\bar{\varepsilon}_1 = 0.32$, bottom subplot). The parameters used in the simulations are otherwise the same as in Figs. 1(a), 2, and 3. The red-vertical line indicates the termination of the drive at $\tau = 12$.

Thresholds

The important dynamical characteristic of the autoresonance is that when starting from zero, the chirped-driven system is captured into resonance only if the driving amplitudes exceed a certain threshold [73]. Thus, if we increase the amplitudes of the drives, the autoresonant excitation of the quasicrystals occurs abruptly, resembling a phase transition.

The thresholds can be analyzed by reducing the problem to the motion of pseudoparticles in an anharmonic slowly varying potential well, similar to the way it was done in Ref. [74] for the single phase weakly nonlinear theory. However, unlike the threshold for the autoresonance of a single phase ion acoustic wave (see Ref. [67]), the general analytical result for the double autoresonance thresholds is difficult to obtain and the thresholds are complicated functions of α_1, α_2, $a(k_1)$, $b(k_1, k_2)$, $c(k_2)$. Nonetheless, it is possible to find the thresholds numerically. As an example let us use the same parameters as in Figs. 1(a), 2, 3, and 4, fix the value of $\bar{\varepsilon}_1$, and solve numerically both the fully and weakly nonlinear equations while sweeping through values of $\bar{\varepsilon}_2$. The results of these simulations are presented in Figs. 7 and 8. Figure 7 shows a colormap of the electron density $n_e(x, \tau) \approx e^{\varphi(x,\tau)}$ obtained by solving the fully nonlinear equations (1)–(3) for various values of $\bar{\varepsilon}_2$: just above the threshold at $\bar{\varepsilon}_2 = 0.338\bar{\varepsilon}_1$ (top subplot), just below the threshold at $\bar{\varepsilon}_2 = 0.337\bar{\varepsilon}_1$ (middle subplot), and below the threshold at $\bar{\varepsilon}_2 = 0.32\bar{\varepsilon}_1$ (bottom subplot), while Fig. 8 shows a colormap of the electron density $n_e(x, \tau) \approx e^{\varphi(x,\tau)}$ obtained by solving the weakly nonlinear equations (38)–(41) for various values of $\bar{\varepsilon}_2$: just above the threshold ($\bar{\varepsilon}_2/\bar{\varepsilon}_1 = 0.339$, top subplot), just below the threshold ($\bar{\varepsilon}_2/\bar{\varepsilon}_1 = 0.338$, middle subplot), and below the threshold ($\bar{\varepsilon}_2/\bar{\varepsilon}_1 = 0.32$, bottom subplot). We can see from these figures that the crystallization is indeed an abrupt phenomenon akin to a phase transition. For the fully nonlinear simulations the threshold lies between $\bar{\varepsilon}_2/\bar{\varepsilon}_1 = 0.337$ and $\bar{\varepsilon}_2/\bar{\varepsilon}_1 = 0.338$, while for the weakly nonlinear simulations the threshold lies between $\bar{\varepsilon}_2/\bar{\varepsilon}_1 = 0.338$ and $\bar{\varepsilon}_2/\bar{\varepsilon}_1 = 0.339$. Such a good agreement for the value of the threshold is another proof that our weakly nonlinear theory is applicable. To better illustrate the threshold nature of the double autoresonance we also produced an animation showing the crystallization of a

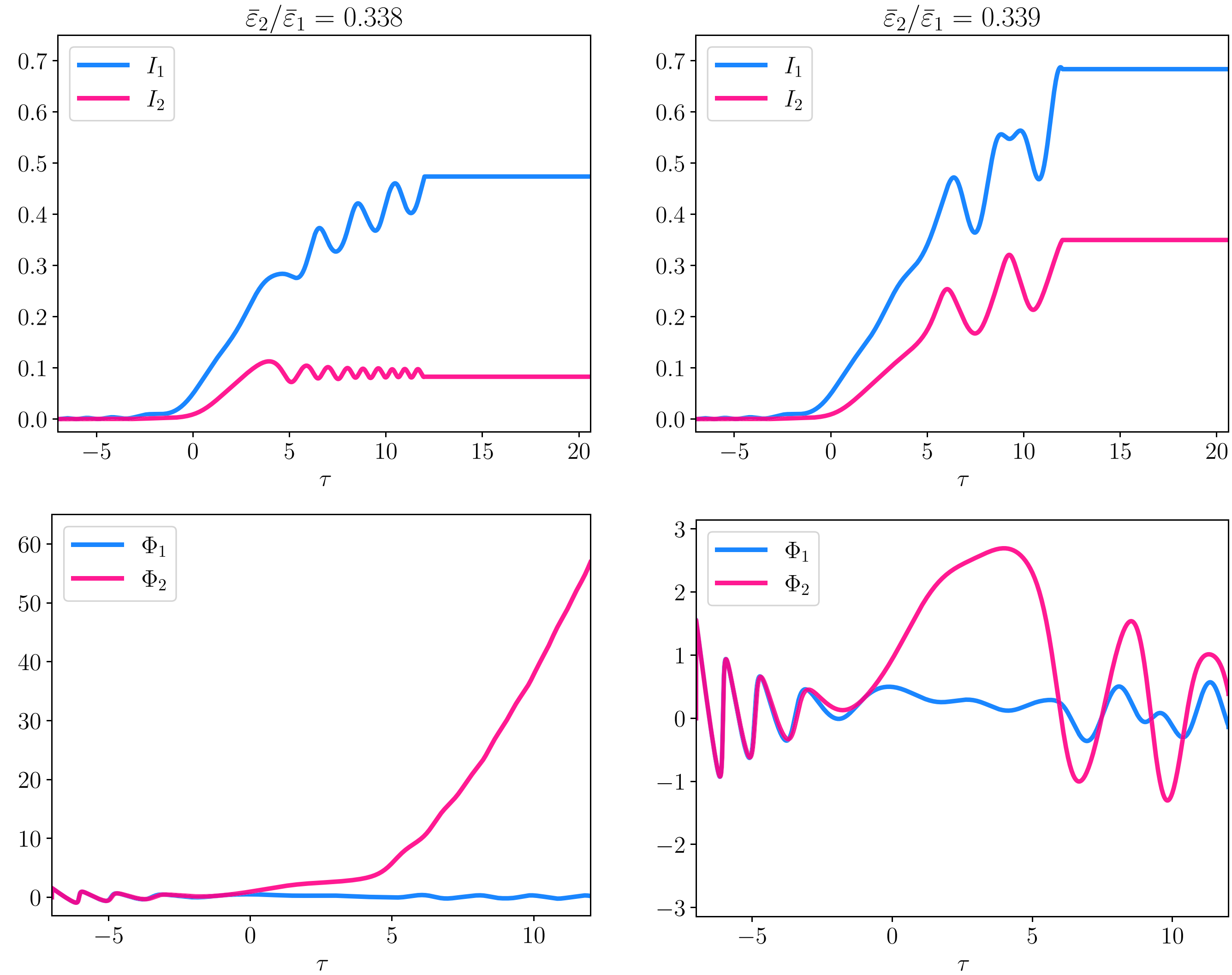

FIG. 9. The effective actions I_1, I_2 (top subplots) and the phase mismatches Φ_1, Φ_2 (bottom subplots) vs slow time $\tau = \sqrt{\alpha_1}t$ obtained by solving the weakly nonlinear reduced dynamical equations (38)–(41). The parameters used in the simulations are the same as in Figs. 1(a), 2, and 3 except for parameter $\bar{\varepsilon}_2$, which is equal to $\bar{\varepsilon}_2 = 0.338\bar{\varepsilon}_1$ (left side) and $\bar{\varepsilon}_2 = 0.339\bar{\varepsilon}_1$ (right side).

single phase structure into a two-phase structure around the threshold as we sweep $\bar{\varepsilon}_2$ from $\bar{\varepsilon}_2 = 0.32\bar{\varepsilon}_1$ to $\bar{\varepsilon}_2 = 0.35\bar{\varepsilon}_1$. The animation is available in the Supplemental Material [75].

The necessity of the phase locking for the autoresonance is demonstrated in Fig. 9, which shows the effective actions I_1, I_2 and the phase mismatches Φ_1, Φ_2 as functions of slow time $\tau = \sqrt{\alpha_1}t$ just below the threshold ($\bar{\varepsilon}_2/\bar{\varepsilon}_1 = 0.338$, left side) and just above the threshold ($\bar{\varepsilon}_2/\bar{\varepsilon}_1 = 0.339$, right side). One can clearly see that just below the threshold the second action I_2 does not enter the autoresonant regime and the growth of the amplitude saturates, while the phase mismatch Φ_2 increases with time signifying the absence of phase locking. In contrast, just above the threshold both phases are locked and the amplitudes I_1, I_2 increase in time similar to the case shown in Fig. 4.

V. CONCLUSIONS

We have demonstrated by means of nonlinear numerical simulations that it is possible to create quasicrystalline spatiotemporal structures in plasma by exciting large amplitude two-phase ion acoustic waves nonlinearly phased locked into the corresponding small amplitude traveling wave drives with chirped frequencies. We have used the Lagrangian formulation and Whitham's averaged variational method to derive analytical results describing the weakly nonlinear evolution of the system. We have applied the weakly nonlinear analytical theory to determine the parameters necessary for the successful excitation and control of multiphase waves. The nonlinearly excited quasicrystalline structures remain even after we turn off the drive. Thus, the space-time quasicrystalline structure in plasma can be excited and then used independently for the purpose of plasma photonics experiments. While our warm fluid model does not have dissipation or noise due to collisions or Landau damping, for example, and, generally speaking, its long-time stability must be addressed by kinetic or particle-in-cell (PIC) simulations, it is apparent that, depending on the time scales of the problem, this structure can be considered as at least a dissipative space-time crystal. We also note that we do not address in this paper whether the driven space-time crystal is a "true" time crystal in the sense of spontaneous symmetry breaking as proposed in Refs. [76,77]; for more discussion regarding this see Refs. [35,78,79].

It is expected that, using our technique, similar structures can be driven in other systems, for example dust acoustic waves in complex plasmas [80]. We expect that multiphase solutions when the number of drives exceeds two are also possible; however, it will be harder to analyze such a system analytically. Finally, we point out that beyond any practical application as a plasma photonic (or accelerating) structure, the possibility of exciting multiphase solutions for in general non-integrable warm ion acoustic waves system is in itself an important fundamental result in the field of nonlinear dynamics. These techniques developed for the excitation of large amplitude ion acoustic waves may be applied to other partial differential equation systems that can support multiphase nonlinear waves.

ACKNOWLEDGMENTS

This work was supported by NSF-BSF Grant No. 1803874 and US-Israel Binational Science Foundation Grant No. 2020233.

APPENDIX A: THE AVERAGED LAGRANGIAN DENSITY

The averaged Lagrangian density

$$\bar{L} = \langle L(\theta_1, \theta_2, t)\rangle_{\theta_1,\theta_2} = \int L(\theta_1, \theta_2, t)\frac{d\theta_1}{2\pi}\frac{d\theta_2}{2\pi} \tag{A1}$$

is equal to the sum of the following terms:

$$\left\langle \frac{1}{2}\varphi_x^2\right\rangle_{\theta_1,\theta_2} = \frac{1}{4}k_1^2C_{10}^2 + \frac{1}{4}k_2^2C_{01}^2 + \frac{1}{4}(k_1+k_2)^2C_{11}^2 + \frac{1}{4}(k_1-k_2)^2C_{1,-1}^2 + k_1^2C_{20}^2 + k_2^2C_{02}^2, \tag{A2}$$

$$\langle \varphi\rangle_{\theta_1,\theta_2} = C_{00}, \tag{A3}$$

$$\left\langle \frac{1}{2}\varphi^2\right\rangle_{\theta_1,\theta_2} = \frac{1}{2}C_{00}^2 + \frac{1}{4}C_{10}^2 + \frac{1}{4}C_{01}^2 + \frac{1}{4}C_{11}^2 + \frac{1}{4}C_{1,-1}^2 + \frac{1}{4}C_{20}^2 + \frac{1}{4}C_{02}^2, \tag{A4}$$

$$\left\langle \frac{1}{6}\varphi^3\right\rangle_{\theta_1,\theta_2} = \frac{1}{4}\left(C_{00} + \frac{1}{2}C_{02}\right)C_{01}^2 + \frac{1}{4}\left(C_{00} + \frac{1}{2}C_{20}\right)C_{10}^2 + \frac{1}{4}(C_{1,-1} + C_{11})C_{01}C_{10}, \tag{A5}$$

$$\left\langle \frac{1}{24}\varphi^4\right\rangle_{\theta_1,\theta_2} = \frac{1}{64}C_{01}^4 + \frac{1}{16}C_{01}^2C_{10}^2 + \frac{1}{64}C_{10}^4, \tag{A6}$$

$$\begin{aligned}\left\langle -\frac{1}{2}(\psi_t\sigma_x + \psi_x\sigma_t)\right\rangle_{\theta_1,\theta_2} &= \frac{1}{2}\omega_1k_1\tilde{B}_{10}\tilde{A}_{10} + \frac{1}{2}\omega_2k_2\tilde{B}_{01}\tilde{A}_{01} + 2\omega_1k_1\tilde{B}_{20}\tilde{A}_{20} + 2\omega_2k_2\tilde{B}_{02}\tilde{A}_{02}\\ &\quad + \frac{1}{2}(\omega_1-\omega_2)(k_1-k_2)\tilde{B}_{1,-1}\tilde{A}_{1,-1} + \frac{1}{2}(\omega_1+\omega_2)(k_1+k_2)\tilde{B}_{11}\tilde{A}_{11},\end{aligned} \tag{A7}$$

$$\begin{aligned}\left\langle -\left(\frac{1}{2}\psi_x^2 + \varphi\right)(1+\sigma_x)\right\rangle_{\theta_1,\theta_2} &= -C_{00} - \frac{1}{4}k_1^2\tilde{B}_{10}^2 - \frac{1}{4}k_2^2\tilde{B}_{01}^2 - k_1^2\tilde{B}_{20}^2 - k_2^2\tilde{B}_{02}^2 - \frac{1}{4}(k_1+k_2)^2\tilde{B}_{11}^2 - \frac{1}{4}(k_1-k_2)^2\tilde{B}_{1,-1}^2\\ &\quad - k_1\left(\frac{1}{2}C_{10}\tilde{A}_{10} + C_{20}\tilde{A}_{20}\right) - k_2\left(\frac{1}{2}C_{01}\tilde{A}_{01} + C_{02}\tilde{A}_{02}\right)\\ &\quad - \frac{1}{2}(k_1+k_2)C_{11}\tilde{A}_{11} - \frac{1}{2}(k_1-k_2)C_{1,-1}\tilde{A}_{1,-1}\\ &\quad - \frac{1}{2}k_2^3\left(\tilde{A}_{01}\tilde{B}_{01}\tilde{B}_{02} + \frac{1}{2}\tilde{A}_{02}\tilde{B}_{01}^2\right) - \frac{1}{2}k_1^3\left(\tilde{A}_{10}\tilde{B}_{10}\tilde{B}_{20} + \frac{1}{2}\tilde{A}_{20}\tilde{B}_{10}^2\right)\\ &\quad - \frac{1}{4}k_1k_2(k_1-k_2)(\tilde{A}_{01}\tilde{B}_{10}\tilde{B}_{1,-1} + \tilde{A}_{1,-1}\tilde{B}_{01}\tilde{B}_{10} + \tilde{A}_{10}\tilde{B}_{01}\tilde{B}_{1,-1})\\ &\quad - \frac{1}{4}k_1k_2(k_1+k_2)(\tilde{A}_{01}\tilde{B}_{11}\tilde{B}_{10} + \tilde{A}_{10}\tilde{B}_{01}\tilde{B}_{11} + \tilde{A}_{11}\tilde{B}_{01}\tilde{B}_{10}),\end{aligned} \tag{A8}$$

$$\begin{aligned}\left\langle -\frac{\Delta^2}{2}\sigma_x^2\left(1+\frac{1}{3}\sigma_x\right)\right\rangle_{\theta_1,\theta_2} &= -\frac{\Delta^2}{4}k_1^2\tilde{A}_{10}^2 - \frac{\Delta^2}{4}k_1^3\tilde{A}_{10}^2\tilde{A}_{20} - \Delta^2k_1^2\tilde{A}_{20}^2 - \frac{\Delta^2}{4}k_2^2\tilde{A}_{01}^2 - \frac{\Delta^2}{4}k_2^3\tilde{A}_{01}^2\tilde{A}_{02} - \Delta^2k_2^2\tilde{A}_{02}^2\\ &\quad - \frac{\Delta^2}{4}k_1k_2(k_1-k_2)\tilde{A}_{01}\tilde{A}_{10}\tilde{A}_{1,-1} - \frac{\Delta^2}{4}k_1k_2(k_1+k_2)\tilde{A}_{01}\tilde{A}_{10}\tilde{A}_{11}\\ &\quad - \frac{\Delta^2}{4}(k_1-k_2)^2\tilde{A}_{1,-1}^2 - \frac{\Delta^2}{4}(k_1+k_2)^2\tilde{A}_{11}^2,\end{aligned} \tag{A9}$$

$$\langle \varphi\varphi_d\rangle_{\theta_1,\theta_2} = \frac{\varepsilon_1}{2}C_{10}\cos(\Phi_1) + \frac{\varepsilon_2}{2}C_{01}\cos(\Phi_2). \tag{A10}$$

APPENDIX B: THE VARIATIONS AND THE AMPLITUDES

In this Appendix we calculate the variations of the averaged Lagrangian with respect to the various amplitudes and express all the second-order amplitudes $\tilde{A}_{20}, \tilde{A}_{02}, \tilde{B}_{20}, \tilde{B}_{02}, C_{20}, C_{02}, \tilde{A}_{11}, \tilde{A}_{1,-1}, \tilde{B}_{11}, \tilde{B}_{1,-1}, C_{11}, C_{1,-1}$ through the first-order amplitudes C_{10} and C_{01}.

To express the second-order amplitudes through C_{10} and C_{01} let us first calculate the variations of the averaged Lagrangian density with respect to the second-order amplitudes:

$$\frac{\partial \bar{L}}{\partial C_{00}} = C_{00} + \frac{1}{4}C_{01}^2 + \frac{1}{4}C_{10}^2 = 0, \tag{B1}$$

$$\frac{\partial \bar{L}}{\partial C_{20}} = 2k_1^2 C_{20} + \frac{1}{2}C_{20} + \frac{1}{8}C_{10}^2 - k_1\tilde{A}_{20} = 0, \tag{B2}$$

$$\frac{\partial \bar{L}}{\partial C_{02}} = 2k_2^2 C_{02} + \frac{1}{2}C_{02} + \frac{1}{8}C_{01}^2 - k_2\tilde{A}_{02} = 0, \tag{B3}$$

$$\frac{\partial \bar{L}}{\partial C_{11}} = \frac{1}{2}(k_1+k_2)^2 C_{11} + \frac{1}{2}C_{11} + \frac{1}{4}C_{01}C_{10} - \frac{1}{2}(k_1+k_2)\tilde{A}_{11} = 0, \tag{B4}$$

$$\frac{\partial \bar{L}}{\partial C_{1,-1}} = \frac{1}{2}(k_1-k_2)^2 C_{1,-1} + \frac{1}{2}C_{1,-1} + \frac{1}{4}C_{01}C_{10} - \frac{1}{2}(k_1-k_2)\tilde{A}_{1,-1} = 0, \tag{B5}$$

$$\frac{\partial \bar{L}}{\partial \tilde{A}_{20}} = 2\omega_1 k_1\tilde{B}_{20} - k_1 C_{20} - \frac{1}{4}k_1^3\tilde{B}_{10}^2 - \frac{\Delta^2}{4}k_1^3\tilde{A}_{10}^2 - 2\Delta^2 k_1^2\tilde{A}_{20} = 0, \tag{B6}$$

$$\frac{\partial \bar{L}}{\partial \tilde{A}_{02}} = 2\omega_2 k_2\tilde{B}_{02} - k_2 C_{02} - \frac{1}{4}k_2^3\tilde{B}_{01}^2 - \frac{\Delta^2}{4}k_2^3\tilde{A}_{01}^2 - 2\Delta^2 k_2^2\tilde{A}_{02} = 0, \tag{B7}$$

$$\frac{\partial \bar{L}}{\partial \tilde{A}_{11}} = \frac{1}{2}(\omega_1+\omega_2)(k_1+k_2)\tilde{B}_{11} - \frac{1}{2}(k_1+k_2)C_{11} - \frac{1}{4}k_1k_2(k_1+k_2)\tilde{B}_{01}\tilde{B}_{10} - \frac{\Delta^2}{4}k_1k_2(k_1+k_2)\tilde{A}_{01}\tilde{A}_{10} - \frac{\Delta^2}{2}(k_1+k_2)^2\tilde{A}_{11} = 0, \tag{B8}$$

$$\frac{\partial \bar{L}}{\partial \tilde{A}_{1,-1}} = \frac{1}{2}(\omega_1-\omega_2)(k_1-k_2)\tilde{B}_{1,-1} - \frac{1}{2}(k_1-k_2)C_{1,-1} - \frac{1}{4}k_1k_2(k_1-k_2)\tilde{B}_{01}\tilde{B}_{10} - \frac{\Delta^2}{4}k_1k_2(k_1-k_2)\tilde{A}_{01}\tilde{A}_{10} - \frac{\Delta^2}{2}(k_1-k_2)^2\tilde{A}_{1,-1} = 0, \tag{B9}$$

$$\frac{\partial \bar{L}}{\partial \tilde{B}_{20}} = 2\omega_1 k_1\tilde{A}_{20} - 2k_1^2\tilde{B}_{20} - \frac{1}{2}k_1^3\tilde{A}_{10}\tilde{B}_{10} = 0, \tag{B10}$$

$$\frac{\partial \bar{L}}{\partial \tilde{B}_{02}} = 2\omega_2 k_2\tilde{A}_{02} - 2k_2^2\tilde{B}_{02} - \frac{1}{2}k_2^3\tilde{A}_{01}\tilde{B}_{01} = 0, \tag{B11}$$

$$\frac{\partial \bar{L}}{\partial \tilde{B}_{11}} = \frac{1}{2}(\omega_1+\omega_2)(k_1+k_2)\tilde{A}_{11} - \frac{1}{2}(k_1+k_2)^2\tilde{B}_{11} - \frac{1}{4}k_1k_2(k_1+k_2)(\tilde{A}_{01}\tilde{B}_{10} + \tilde{A}_{10}\tilde{B}_{01}) = 0, \tag{B12}$$

$$\frac{\partial \bar{L}}{\partial \tilde{B}_{1,-1}} = \frac{1}{2}(\omega_1-\omega_2)(k_1-k_2)\tilde{A}_{1,-1} - \frac{1}{2}(k_1-k_2)^2\tilde{B}_{1,-1} - \frac{1}{4}k_1k_2(k_1-k_2)(\tilde{A}_{01}\tilde{B}_{10} + \tilde{A}_{10}\tilde{B}_{01}) = 0. \tag{B13}$$

From Eq. (B1) we obtain

$$C_{00} = -\tfrac{1}{4}C_{01}^2 - \tfrac{1}{4}C_{10}^2. \tag{B14}$$

From Eqs. (B2), (B3), (B6), (B7), (B10), and (B11) we obtain

$$\tilde{A}_{20} = \frac{k_1^3(4k_1^2+1)\tilde{B}_{10}^2 + 2\omega_1 k_1^2(4k_1^2+1)\tilde{A}_{10}\tilde{B}_{10} - k_1 C_{10}^2 + \Delta^2 k_1^3(4k_1^2+1)\tilde{A}_{10}^2}{8\left[(\omega_1^2 - \Delta^2 k_1^2)(4k_1^2+1) - k_1^2\right]}, \tag{B15}$$

$$\tilde{A}_{02} = \frac{k_2^3(4k_2^2+1)\tilde{B}_{01}^2 + 2\omega_2 k_2^2(4k_2^2+1)\tilde{A}_{01}\tilde{B}_{01} - k_2 C_{01}^2 + \Delta^2 k_2^3(4k_2^2+1)\tilde{A}_{01}^2}{8\left[(\omega_2^2 - \Delta^2 k_2^2)(4k_2^2+1) - k_2^2\right]}, \tag{B16}$$

$$\tilde{B}_{20} = \frac{\omega_1 k_1^2(4k_1^2+1)\tilde{B}_{10}^2 + 2k_1^3\tilde{A}_{10}\tilde{B}_{10} - \omega_1 C_{10}^2 + \Delta^2\omega_1 k_1^2(4k_1^2+1)\tilde{A}_{10}^2 + 2\Delta^2 k_1^3(4k_1^2+1)\tilde{A}_{10}\tilde{B}_{10}}{8\left[(\omega_1^2 - \Delta^2 k_1^2)(4k_1^2+1) - k_1^2\right]}, \tag{B17}$$

$$\tilde{B}_{02} = \frac{\omega_2 k_2^2(4k_2^2+1)\tilde{B}_{01}^2 + 2k_2^3\tilde{A}_{01}\tilde{B}_{01} - \omega_2 C_{01}^2 + \Delta^2\omega_2 k_2^2(4k_2^2+1)\tilde{A}_{01}^2 + 2\Delta^2 k_2^3(4k_2^2+1)\tilde{A}_{01}\tilde{B}_{01}}{8\left[(\omega_2^2 - \Delta^2 k_2^2)(4k_2^2+1) - k_2^2\right]}, \tag{B18}$$

$$C_{20} = \frac{k_1^4\tilde{B}_{10}^2 + 2\omega_1 k_1^3\tilde{A}_{10}\tilde{B}_{10} - \omega_1^2 C_{10}^2 + \Delta^2 k_1^4\tilde{A}_{10}^2 + \Delta^2 k_1^2 C_{10}^2}{4\left[(\omega_1^2 - \Delta^2 k_1^2)(4k_1^2+1) - k_1^2\right]}, \tag{B19}$$

$$C_{02} = \frac{k_2^4\tilde{B}_{01}^2 + 2\omega_2 k_2^3\tilde{A}_{01}\tilde{B}_{01} - \omega_2^2 C_{01}^2 + \Delta^2 k_2^4\tilde{A}_{01}^2 + \Delta^2 k_2^2 C_{01}^2}{4\left[(\omega_2^2 - \Delta^2 k_2^2)(4k_2^2+1) - k_2^2\right]}. \tag{B20}$$

From Eqs. (B4), (B5), (B8), (B9), (B12), and (B13) we obtain

$$\tilde{A}_{11} = \frac{k_1k_2(k_1+k_2)[(k_1+k_2)^2+1]\tilde{B}_{01}\tilde{B}_{10} - (k_1+k_2)C_{01}C_{10}}{2\{[(\omega_1+\omega_2)^2 - \Delta^2(k_1+k_2)^2][(k_1+k_2)^2+1] - (k_1+k_2)^2\}} + \frac{(\omega_1+\omega_2)k_1k_2[(k_1+k_2)^2+1](\tilde{A}_{01}\tilde{B}_{10} + \tilde{A}_{10}\tilde{B}_{01})}{2\{[(\omega_1+\omega_2)^2 - \Delta^2(k_1+k_2)^2][(k_1+k_2)^2+1] - (k_1+k_2)^2\}}$$

$$+\frac{\Delta^2 k_1k_2(k_1+k_2)[(k_1+k_2)^2+1]\tilde{A}_{01}\tilde{A}_{10}}{2\{[(\omega_1+\omega_2)^2-\Delta^2(k_1+k_2)^2][(k_1+k_2)^2+1]-(k_1+k_2)^2\}}, \tag{B21}$$

$$\tilde{A}_{1,-1}=\frac{k_1k_2(k_1-k_2)[(k_1-k_2)^2+1]\tilde{B}_{01}\tilde{B}_{10}-(k_1-k_2)C_{01}C_{10}}{2\{[(\omega_1-\omega_2)^2-\Delta^2(k_1-k_2)^2][(k_1-k_2)^2+1]-(k_1-k_2)^2\}}$$
$$+\frac{(\omega_1-\omega_2)k_1k_2[(k_1-k_2)^2+1](\tilde{A}_{01}\tilde{B}_{10}+\tilde{A}_{10}\tilde{B}_{01})}{2\{[(\omega_1-\omega_2)^2-\Delta^2(k_1-k_2)^2][(k_1-k_2)^2+1]-(k_1-k_2)^2\}}$$
$$+\frac{\Delta^2 k_1k_2(k_1-k_2)[(k_1-k_2)^2+1]\tilde{A}_{01}\tilde{A}_{10}}{2\{[(\omega_1-\omega_2)^2-\Delta^2(k_1-k_2)^2][(k_1-k_2)^2+1]-(k_1-k_2)^2\}}, \tag{B22}$$

$$\tilde{B}_{11}=\frac{(\omega_1+\omega_2)k_1k_2[(k_1+k_2)^2+1]\tilde{B}_{01}\tilde{B}_{10}-(\omega_1+\omega_2)C_{01}C_{10}+k_1k_2(k_1+k_2)(\tilde{A}_{01}\tilde{B}_{10}+\tilde{A}_{10}\tilde{B}_{01})}{2\{[(\omega_1+\omega_2)^2-\Delta^2(k_1+k_2)^2][(k_1+k_2)^2+1]-(k_1+k_2)^2\}}$$
$$+\frac{\Delta^2 k_1k_2[(k_1+k_2)^2+1][(\omega_1+\omega_2)\tilde{A}_{01}\tilde{A}_{10}+(k_1+k_2)(\tilde{A}_{01}\tilde{B}_{10}+\tilde{A}_{10}\tilde{B}_{01})]}{2\{[(\omega_1+\omega_2)^2-\Delta^2(k_1+k_2)^2][(k_1+k_2)^2+1]-(k_1+k_2)^2\}}, \tag{B23}$$

$$\tilde{B}_{1,-1}=\frac{(\omega_1-\omega_2)k_1k_2[(k_1-k_2)^2+1]\tilde{B}_{01}\tilde{B}_{10}-(\omega_1-\omega_2)C_{01}C_{10}+k_1k_2(k_1-k_2)(\tilde{A}_{01}\tilde{B}_{10}+\tilde{A}_{10}\tilde{B}_{01})}{2\{[(\omega_1-\omega_2)^2-\Delta^2(k_1-k_2)^2][(k_1-k_2)^2+1]-(k_1-k_2)^2\}}$$
$$+\frac{\Delta^2 k_1k_2[(k_1-k_2)^2+1][(\omega_1-\omega_2)\tilde{A}_{01}\tilde{A}_{10}+(k_1-k_2)(\tilde{A}_{01}\tilde{B}_{10}+\tilde{A}_{10}\tilde{B}_{01})]}{2\{[(\omega_1-\omega_2)^2-\Delta^2(k_1-k_2)^2][(k_1-k_2)^2+1]-(k_1-k_2)^2\}}, \tag{B24}$$

$$C_{11}=\frac{k_1k_2(k_1+k_2)^2\tilde{B}_{01}\tilde{B}_{10}-(\omega_1+\omega_2)^2C_{01}C_{10}+(\omega_1+\omega_2)k_1k_2(k_1+k_2)(\tilde{A}_{01}\tilde{B}_{10}+\tilde{A}_{10}\tilde{B}_{01})}{2\{[(\omega_1+\omega_2)^2-\Delta^2(k_1+k_2)^2][(k_1+k_2)^2+1]-(k_1+k_2)^2\}}$$
$$+\frac{\Delta^2(k_1+k_2)^2(C_{01}C_{10}+k_1k_2\tilde{A}_{01}\tilde{A}_{10})}{2\{[(\omega_1+\omega_2)^2-\Delta^2(k_1+k_2)^2][(k_1+k_2)^2+1]-(k_1+k_2)^2\}}, \tag{B25}$$

$$C_{1,-1}=\frac{k_1k_2(k_1-k_2)^2\tilde{B}_{01}\tilde{B}_{10}-(\omega_1-\omega_2)^2C_{01}C_{10}+(\omega_1-\omega_2)k_1k_2(k_1-k_2)(\tilde{A}_{01}\tilde{B}_{10}+\tilde{A}_{10}\tilde{B}_{01})}{2\{[(\omega_1-\omega_2)^2-\Delta^2(k_1-k_2)^2][(k_1-k_2)^2+1]-(k_1-k_2)^2\}}$$
$$+\frac{\Delta^2(k_1-k_2)^2(C_{01}C_{10}+k_1k_2\tilde{A}_{01}\tilde{A}_{10})}{2\{[(\omega_1-\omega_2)^2-\Delta^2(k_1-k_2)^2][(k_1-k_2)^2+1]-(k_1-k_2)^2\}}. \tag{B26}$$

Finally, by using Eqs. (20)–(23), we can express all the second-order amplitudes through C_{10} and C_{01}:

$$\tilde{A}_{20}=\frac{k_1}{8}\frac{k_1^2(3\omega_1^2+\Delta^2k_1^2)(4k_1^2+1)-(\omega_1^2-\Delta^2k_1^2)^2}{(\omega_1^2-\Delta^2k_1^2)^2[(\omega_1^2-\Delta^2k_1^2)(4k_1^2+1)-k_1^2]}C_{10}^2, \tag{B27}$$

$$\tilde{A}_{02}=\frac{k_2}{8}\frac{k_2^2(3\omega_2^2+\Delta^2k_2^2)(4k_2^2+1)-(\omega_2^2-\Delta^2k_2^2)^2}{(\omega_2^2-\Delta^2k_2^2)^2[(\omega_2^2-\Delta^2k_2^2)(4k_2^2+1)-k_2^2]}C_{01}^2, \tag{B28}$$

$$\tilde{B}_{20}=\frac{\omega_1}{8}\frac{k_1^2(\omega_1^2+3\Delta^2k_1^2)(4k_1^2+1)+2k_1^4-(\omega_1^2-\Delta^2k_1^2)^2}{(\omega_1^2-\Delta^2k_1^2)^2[(\omega_1^2-\Delta^2k_1^2)(4k_1^2+1)-k_1^2]}C_{10}^2, \tag{B29}$$

$$\tilde{B}_{02}=\frac{\omega_2}{8}\frac{k_2^2(\omega_2^2+3\Delta^2k_2^2)(4k_2^2+1)+2k_2^4-(\omega_2^2-\Delta^2k_2^2)^2}{(\omega_2^2-\Delta^2k_2^2)^2[(\omega_2^2-\Delta^2k_2^2)(4k_2^2+1)-k_2^2]}C_{01}^2, \tag{B30}$$

$$C_{20}=\frac{k_1^4(3\omega_1^2+\Delta^2k_1^2)-(\omega_1^2-\Delta^2k_1^2)^3}{4(\omega_1^2-\Delta^2k_1^2)^2[(\omega_1^2-\Delta^2k_1^2)(4k_1^2+1)-k_1^2]}C_{10}^2, \tag{B31}$$

$$C_{02}=\frac{k_2^4(3\omega_2^2+\Delta^2k_2^2)-(\omega_2^2-\Delta^2k_2^2)^3}{4(\omega_2^2-\Delta^2k_2^2)^2[(\omega_2^2-\Delta^2k_2^2)(4k_2^2+1)-k_2^2]}C_{01}^2, \tag{B32}$$

$$\tilde{A}_{11}=\frac{k_1k_2[(\omega_1\omega_2+\Delta^2k_1k_2)(k_1+k_2)+(\omega_1+\omega_2)(k_2\omega_1+k_1\omega_2)][(k_1+k_2)^2+1]}{2(\omega_1^2-\Delta^2k_1^2)(\omega_2^2-\Delta^2k_2^2)\{[(\omega_1+\omega_2)^2-\Delta^2(k_1+k_2)^2][(k_1+k_2)^2+1]-(k_1+k_2)^2\}}C_{01}C_{10}$$
$$-\frac{k_1+k_2}{2\{[(\omega_1+\omega_2)^2-\Delta^2(k_1+k_2)^2][(k_1+k_2)^2+1]-(k_1+k_2)^2\}}C_{01}C_{10}, \tag{B33}$$

$$\tilde{A}_{1,-1}=\frac{k_1k_2[(\omega_1\omega_2+\Delta^2k_1k_2)(k_1-k_2)+(\omega_1-\omega_2)(k_2\omega_1+k_1\omega_2)][(k_1-k_2)^2+1]}{2(\omega_1^2-\Delta^2k_1^2)(\omega_2^2-\Delta^2k_2^2)\{[(\omega_1-\omega_2)^2-\Delta^2(k_1-k_2)^2][(k_1-k_2)^2+1]-(k_1-k_2)^2\}}C_{01}C_{10}$$
$$-\frac{k_1-k_2}{2\{[(\omega_1-\omega_2)^2-\Delta^2(k_1-k_2)^2][(k_1-k_2)^2+1]-(k_1-k_2)^2\}}C_{01}C_{10}, \tag{B34}$$

$$\tilde{B}_{11} = \frac{k_1k_2\{[(\omega_1+\omega_2)(\omega_1\omega_2+\Delta^2k_1k_2)+\Delta^2(k_1+k_2)(k_2\omega_1+k_1\omega_2)][(k_1+k_2)^2+1]+(k_1+k_2)(k_2\omega_1+k_1\omega_2)\}}{2(\omega_1^2-\Delta^2k_1^2)(\omega_2^2-\Delta^2k_2^2)\{[(\omega_1+\omega_2)^2-\Delta^2(k_1+k_2)^2][(k_1+k_2)^2+1]-(k_1+k_2)^2\}}C_{01}C_{10}$$
$$-\frac{\omega_1+\omega_2}{2\{[(\omega_1+\omega_2)^2-\Delta^2(k_1+k_2)^2][(k_1+k_2)^2+1]-(k_1+k_2)^2\}}C_{01}C_{10}, \quad \text{(B35)}$$

$$\tilde{B}_{1,-1} = \frac{k_1k_2\{[(\omega_1-\omega_2)(\omega_1\omega_2+\Delta^2k_1k_2)+\Delta^2(k_1-k_2)(k_2\omega_1+k_1\omega_2)][(k_1-k_2)^2+1]+(k_1-k_2)(k_2\omega_1+k_1\omega_2)\}}{2(\omega_1^2-\Delta^2k_1^2)(\omega_2^2-\Delta^2k_2^2)\{[(\omega_1-\omega_2)^2-\Delta^2(k_1-k_2)^2][(k_1-k_2)^2+1]-(k_1-k_2)^2\}}C_{01}C_{10}$$
$$-\frac{\omega_1-\omega_2}{2\{[(\omega_1-\omega_2)^2-\Delta^2(k_1-k_2)^2][(k_1-k_2)^2+1]-(k_1-k_2)^2\}}C_{01}C_{10}, \quad \text{(B36)}$$

$$C_{11} = \frac{k_1k_2(k_1+k_2)[(k_1+k_2)(\omega_1\omega_2+\Delta^2k_1k_2)+(\omega_1+\omega_2)(k_2\omega_1+k_1\omega_2)]}{2(\omega_1^2-\Delta^2k_1^2)(\omega_2^2-\Delta^2k_2^2)\{[(\omega_1+\omega_2)^2-\Delta^2(k_1+k_2)^2][(k_1+k_2)^2+1]-(k_1+k_2)^2\}}C_{01}C_{10}$$
$$-\frac{(\omega_1+\omega_2)^2-\Delta^2(k_1+k_2)^2}{2\{[(\omega_1+\omega_2)^2-\Delta^2(k_1+k_2)^2][(k_1+k_2)^2+1]-(k_1+k_2)^2\}}C_{01}C_{10}, \quad \text{(B37)}$$

$$C_{1,-1} = \frac{k_1k_2(k_1-k_2)[(k_1-k_2)(\omega_1\omega_2+\Delta^2k_1k_2)+(\omega_1-\omega_2)(k_2\omega_1+k_1\omega_2)]}{2(\omega_1^2-\Delta^2k_1^2)(\omega_2^2-\Delta^2k_2^2)\{[(\omega_1-\omega_2)^2-\Delta^2(k_1-k_2)^2][(k_1-k_2)^2+1]-(k_1-k_2)^2\}}C_{01}C_{10}$$
$$-\frac{(\omega_1-\omega_2)^2-\Delta^2(k_1-k_2)^2}{2\{[(\omega_1-\omega_2)^2-\Delta^2(k_1-k_2)^2][(k_1-k_2)^2+1]-(k_1-k_2)^2\}}C_{01}C_{10}. \quad \text{(B38)}$$

Note that in the limiting case of cold ions ($\Delta = 0$) and with two identical counter propagating traveling waves (i.e., a standing wave with $k_1 = -k, k_2 = k, \omega_1 = \omega_2 = \omega, \varepsilon_1 = \varepsilon_2 = \varepsilon$) the above amplitudes coincide with the amplitudes derived in Ref. [60], as expected. In particular, the amplitudes $a_1, a_2, A, b_1, b_2, c_0, c_1, c_2, C$ from Ref. [60] are related to the amplitudes in this paper as follows:

$$\tilde{A}_{10} = -\frac{a_1}{2}, \quad \tilde{A}_{01} = \frac{a_1}{2}, \quad \tilde{A}_{20} = -\frac{a_2}{2}, \quad \tilde{A}_{02} = \frac{a_2}{2}, \quad \tilde{A}_{1,-1} = -A, \quad \text{(B39)}$$

$$\tilde{B}_{10} = -\frac{b_1}{2}, \quad \tilde{B}_{01} = -\frac{b_1}{2}, \quad \tilde{B}_{20} = -\frac{b_2}{2}, \quad \tilde{B}_{02} = -\frac{b_2}{2}, \quad \text{(B40)}$$

$$C_{00} = \frac{c_0}{2}, \quad C_{11} = \frac{c_0}{2}, \quad C_{10} = \frac{c_1}{2}, \quad C_{01} = \frac{c_1}{2}, \quad C_{1,-1} = C, \quad C_{20} = \frac{c_2}{2}, \quad C_{02} = \frac{c_2}{2}. \quad \text{(B41)}$$

To derive weakly nonlinear equations we also need to calculate the variations of $\bar{L}$ with respect to the first-order amplitudes:

$$\frac{\partial \bar{L}}{\partial C_{10}} = -\frac{1}{2}k_1\tilde{A}_{10} + \frac{1}{2}(1+k_1^2)C_{10} + \frac{1}{2}C_{10}\left(\frac{1}{8}C_{10}^2 + \frac{1}{4}C_{01}^2 + C_{00} + \frac{1}{2}C_{20}\right) + \frac{1}{4}C_{01}(C_{1,-1}+C_{11}) + \frac{\varepsilon_1}{2}\cos(\Phi_1) = 0, \quad \text{(B42)}$$

$$\frac{\partial \bar{L}}{\partial C_{01}} = -\frac{1}{2}k_2\tilde{A}_{01} + \frac{1}{2}(1+k_2^2)C_{01} + \frac{1}{2}C_{01}\left(\frac{1}{8}C_{01}^2 + \frac{1}{4}C_{10}^2 + C_{00} + \frac{1}{2}C_{02}\right) + \frac{1}{4}C_{10}(C_{1,-1}+C_{11}) + \frac{\varepsilon_2}{2}\cos(\Phi_2) = 0, \quad \text{(B43)}$$

$$\frac{\partial \bar{L}}{\partial \tilde{B}_{10}} = -\frac{1}{2}k_1^2(1+k_1\tilde{A}_{20})\tilde{B}_{10} - \frac{1}{4}k_1k_2[(k_1-k_2)\tilde{A}_{1,-1}+(k_1+k_2)\tilde{A}_{11}]\tilde{B}_{01}$$
$$+\frac{1}{2}k_1(\omega_1 - k_1^2\tilde{B}_{20})\tilde{A}_{10} - \frac{1}{4}k_1k_2[(k_1-k_2)\tilde{B}_{1,-1}+(k_1+k_2)\tilde{B}_{11}]\tilde{A}_{01} = 0, \quad \text{(B44)}$$

$$\frac{\partial \bar{L}}{\partial \tilde{B}_{01}} = -\frac{1}{2}k_2^2(1+k_2\tilde{A}_{02})\tilde{B}_{01} - \frac{1}{4}k_1k_2[(k_1-k_2)\tilde{A}_{1,-1}+(k_1+k_2)\tilde{A}_{11}]\tilde{B}_{10}$$
$$+\frac{1}{2}k_2(\omega_2 - k_2^2\tilde{B}_{02})\tilde{A}_{01} - \frac{1}{4}k_1k_2[(k_1-k_2)\tilde{B}_{1,-1}+(k_1+k_2)\tilde{B}_{11}]\tilde{A}_{10} = 0, \quad \text{(B45)}$$

$$\frac{\partial \bar{L}}{\partial \tilde{A}_{10}} = -\frac{1}{2}k_1C_{10} + \frac{1}{2}k_1(\omega_1 - k_1^2\tilde{B}_{20})\tilde{B}_{10} - \frac{1}{4}k_1k_2[(k_1-k_2)\tilde{B}_{1,-1}+(k_1+k_2)\tilde{B}_{11}]\tilde{B}_{01}$$
$$-\frac{\Delta^2}{2}k_1^2(1+k_1\tilde{A}_{20})\tilde{A}_{10} - \frac{\Delta^2}{4}k_1k_2[(k_1-k_2)\tilde{A}_{1,-1}+(k_1+k_2)\tilde{A}_{11}]\tilde{A}_{01} = 0, \quad \text{(B46)}$$

$$\frac{\partial \bar{L}}{\partial \tilde{A}_{01}} = -\frac{1}{2}k_2C_{01} + \frac{1}{2}k_2(\omega_2 - k_2^2\tilde{B}_{02})\tilde{B}_{01} - \frac{1}{4}k_1k_2[(k_1-k_2)\tilde{B}_{1,-1}+(k_1+k_2)\tilde{B}_{11}]\tilde{B}_{10}$$
$$-\frac{\Delta^2}{2}k_2^2(1+k_2\tilde{A}_{02})\tilde{A}_{01} - \frac{\Delta^2}{4}k_1k_2[(k_1-k_2)\tilde{A}_{1,-1}+(k_1+k_2)\tilde{A}_{11}]\tilde{A}_{10} = 0. \quad \text{(B47)}$$

APPENDIX C: FUNCTIONS $P(k_1, \omega_1)$ AND $Q(k_1, \omega_1; k_2, \omega_2)$

Function $P(k_1, \omega_1)$ is defined through

$$C_{10}^2 P(k_1, \omega_1) = -\frac{1}{8}C_{10}^2 + \frac{1}{2}C_{20} - \frac{2\omega_1 k_1^4}{\left(\omega_1^2 - \Delta^2 k_1^2\right)^2}\tilde{B}_{20} - \frac{k_1^3\left(\omega_1^2 + \Delta^2 k_1^2\right)}{\left(\omega_1^2 - \Delta^2 k_1^2\right)^2}\tilde{A}_{20}, \tag{C1}$$

or, equivalently due to symmetry, through

$$C_{01}^2 P(k_2, \omega_2) = -\frac{1}{8}C_{01}^2 + \frac{1}{2}C_{02} - \frac{2\omega_2 k_2^4}{\left(\omega_2^2 - \Delta^2 k_2^2\right)^2}\tilde{B}_{02} - \frac{k_2^3\left(\omega_2^2 + \Delta^2 k_2^2\right)}{\left(\omega_2^2 - \Delta^2 k_2^2\right)^2}\tilde{A}_{02}, \tag{C2}$$

while $Q(k_1, \omega_1; k_2, \omega_2)$ is defined through

$$\begin{aligned} C_{01}C_{10}Q(k_1, \omega_1; k_2, \omega_2) = \frac{1}{2}\Bigg\{ & C_{1,-1} + C_{11} - \frac{k_1 k_2(\omega_1\omega_2 + \Delta^2 k_1 k_2)}{\left(\omega_1^2 - \Delta^2 k_1^2\right)\left(\omega_2^2 - \Delta^2 k_2^2\right)}[(k_1 - k_2)\tilde{A}_{1,-1} + (k_1 + k_2)\tilde{A}_{11}] \\ & - \frac{k_1 k_2(k_1\omega_2 + k_2\omega_1)}{\left(\omega_1^2 - \Delta^2 k_1^2\right)\left(\omega_2^2 - \Delta^2 k_2^2\right)}[(k_1 - k_2)\tilde{B}_{1,-1} + (k_1 + k_2)\tilde{B}_{11}]\Bigg\}. \end{aligned} \tag{C3}$$

Here, the amplitudes $\tilde{A}_{20}$, $\tilde{A}_{02}$, $\tilde{B}_{20}$, $\tilde{B}_{02}$, C_{20}, C_{02}, $\tilde{A}_{11}$, $\tilde{A}_{1,-1}$, $\tilde{B}_{11}$, $\tilde{B}_{1,-1}$, C_{11}, $C_{1,-1}$ should be expressed through C_{10}, C_{01}, k_1, k_2, ω_1, ω_2, Δ using Eqs. (B27)–(B38), so that $P(k_1, \omega_1)$, $Q(k_1, \omega_1; k_2, \omega_2)$ are functions of k_1, k_2, ω_1, ω_2, Δ only.

---

[1] J. Joannopoulos, *Photonic Crystals: Molding the Flow of Light (Second Edition)* (Princeton University Press, Princeton, 2008).

[2] K. M. Ho, C. T. Chan, and C. M. Soukoulis, Existence of a Photonic Gap in Periodic Dielectric Structures, Phys. Rev. Lett. **65**, 3152 (1990).

[3] S. John, Strong Localization of Photons in Certain Disordered Dielectric Superlattices, Phys. Rev. Lett. **58**, 2486 (1987).

[4] E. Yablonovitch, Inhibited Spontaneous Emission in Solid-State Physics and Electronics, Phys. Rev. Lett. **58**, 2059 (1987).

[5] H. Hojo and A. Mase, Dispersion relation of electromagnetic waves in one-dimensional plasma photonic crystals, J. Plasma Fusion Res. **80**, 89 (2004).

[6] H. Hojo and A. Mase, Electromagnetic-wave transmittance characteristics in one-dimensional plasma photonic crystals, J. Plasma Fusion Res. SERIES **8**, 477 (2009).

[7] M. Solaimani, Optical transport properties of one dimensional plasma photonic crystals: Crossover from rectangular to semi-sinusoidal layers, Results Phys. **16**, 102843 (2020).

[8] L. Qi, Z. Yang, F. Lan, X. Gao, and Z. Shi, Properties of obliquely incident electromagnetic wave in one-dimensional magnetized plasma photonic crystals, Phys. Plasmas **17**, 042501 (2010).

[9] Z. Rahmani and N. Rezaee, The reflection and absorption characteristics of one-dimensional ternary plasma photonic crystals irradiated by TE and TM waves, Optik **184**, 134 (2019).

[10] W. Li, Y. Zhao, R. Cui, and H. Zhang, Plasma photonic crystal, Front. Optoelectron. China **2**, 103 (2009).

[11] L. Zhang and J.-T. Ouyang, Experiment and simulation on one-dimensional plasma photonic crystals, Phys. Plasmas **21**, 103514 (2014).

[12] O. Sakai, T. Sakaguchi, Y. Ito, and K. Tachibana, Interaction and control of millimetre-waves with microplasma arrays, Plasma Phys. Controlled Fusion **47**, B617 (2005).

[13] O. Sakai and K. Tachibana, Plasmas as metamaterials: A review, Plasma Sources Sci. Technol. **21**, 013001 (2012).

[14] L. Qi, C. Li, G. Fang, and X. Gao, The absorbing properties of two-dimensional plasma photonic crystals, Plasma Sci. Technol. **17**, 4 (2015).

[15] H.-F. Zhang, S.-B. Liu, X.-K. Kong, Chen-Chen, and B.-R. Bian, The properties of photonic band gaps for three-dimensional plasma photonic crystals in a diamond structure, Phys. Plasmas **20**, 042110 (2013).

[16] H.-F. Zhang, S.-B. Liu, and X.-K. Kong, Dispersion properties of three-dimensional plasma photonic crystals in diamond lattice arrangement, J. Lightwave Technol. **31**, 1694 (2013).

[17] K. Suzuki, K. Kitano, K. Ishizaki, and S. Noda, Three-dimensional photonic crystals created by single-step multi-directional plasma etching, Opt. Express **22**, 17099 (2014).

[18] Y. Liang, Z. Liu, L. Lin, J. Peng, R. Liu, and Q. Lin, Transmission characteristics of electromagnetic waves in 2D tunable plasma photonic crystals, Appl. Opt. **60**, 2510 (2021).

[19] B. Wang and M. A. Cappelli, A plasma photonic crystal bandgap device, Appl. Phys. Lett. **108**, 161101 (2016).

[20] D. Levine and P. J. Steinhardt, Quasicrystals: A New Class of Ordered Structures, Phys. Rev. Lett. **53**, 2477 (1984).

[21] P. N. Dyachenko, V. S. Pavelyev, and V. A. Soifer, Graded photonic quasicrystals, Opt. Lett. **37**, 2178 (2012).

[22] A. Poddubny and E. Ivchenko, Photonic quasicrystalline and aperiodic structures, Phys. E **42**, 1871 (2010).

[23] R. Lifshitz, A. Arie, and A. Bahabad, Photonic Quasicrystals for Nonlinear Optical Frequency Conversion, Phys. Rev. Lett. **95**, 133901 (2005).

[24] Z. V. Vardeny, A. Nahata, and A. Agrawal, Optics of photonic quasicrystals, Nat. Photonics **7**, 177 (2013).

[25] A. Bahabad, A. Ganany-Padowicz, and A. Arie, Engineering two-dimensional nonlinear photonic quasi-crystals, Opt. Lett. **33**, 1386 (2008).

[26] B. Freedman, G. Bartal, M. Segev, R. Lifshitz, D. N. Christodoulides, and J. W. Fleischer, Wave and defect dynamics

in nonlinear photonic quasicrystals, Nature (London) **440**, 1166 (2006).
[27] Y. Neve-Oz, T. Pollok, S. Burger, M. Golosovsky, and D. Davidov, Resonant transmission of electromagnetic waves through two-dimensional photonic quasicrystals, J. Appl. Phys. **107**, 063105 (2010).
[28] Y. S. Chan, C. T. Chan, and Z. Y. Liu, Photonic Band Gaps in Two Dimensional Photonic Quasicrystals, Phys. Rev. Lett. **80**, 956 (1998).
[29] E. Lustig, Y. Sharabi, and M. Segev, Topological aspects of photonic time crystals, Optica **5**, 1390 (2018).
[30] J. R. Zurita-Sánchez, P. Halevi, and J. C. Cervantes-González, Reflection and transmission of a wave incident on a slab with a time-periodic dielectric function $\mu(t)$, Phys. Rev. A **79**, 053821 (2009).
[31] J. R. Zurita-Sánchez, J. H. Abundis-Patiño, and P. Halevi, Pulse propagation through a slab with time-periodic dielectric function ϵ(t), Opt. Express **20**, 5586 (2012).
[32] J. R. Zurita-Sánchez and P. Halevi, Resonances in the optical response of a slab with time-periodic dielectric function $\epsilon(t)$, Phys. Rev. A **81**, 053834 (2010).
[33] M. A. Salem and C. Caloz, Temporal photonic crystals: Causality versus periodicity, in *2015 International Conference on Electromagnetics in Advanced Applications (ICEAA)* (IEEE, Turin, Italy, 2015) pp. 490–493.
[34] J. S. Martínez-Romero and P. Halevi, Parametric resonances in a temporal photonic crystal slab, Phys. Rev. A **98**, 053852 (2018).
[35] K. Sacha, Photonic time crystals, in *Time Crystals* (Springer International Publishing, Cham, 2020) pp. 251–265.
[36] N. Wang, Z.-Q. Zhang, and C. T. Chan, Photonic floquet media with a complex time-periodic permittivity, Phys. Rev. B **98**, 085142 (2018).
[37] J. Park and B. Min, Spatiotemporal plane wave expansion method for arbitrary space–time periodic photonic media, Opt. Lett. **46**, 484 (2021).
[38] F. Biancalana, A. Amann, A. V. Uskov, and E. P. O'Reilly, Dynamics of light propagation in spatiotemporal dielectric structures, Phys. Rev. E **75**, 046607 (2007).
[39] F. Biancalana, A. Amann, and E. P. O'Reilly, Gap solitons in spatiotemporal photonic crystals, Phys. Rev. A **77**, 011801(R) (2008).
[40] L. Zeng, J. Xu, C. Wang, J. Zhang, Y. Zhao, J. Zeng, and R. Song, Photonic time crystals, Sci. Rep. **7**, 17165 (2017).
[41] C. Caloz and Z.-L. Deck-Léger, Spacetime metamaterials—Part I: General concepts, IEEE Trans. Antennas Propag. **68**, 1569 (2020).
[42] C. Caloz and Z.-L. Deck-Léger, Spacetime metamaterials—Part II: Theory and applications, IEEE Trans. Antennas Propag. **68**, 1583 (2020).
[43] Y. Sharabi, E. Lustig, A. Dikopoltsev, Y. Lumer, and M. Segev, Spatiotemporal photonic crystals, in *2020 Conference on Lasers and Electro-Optics (CLEO)* (Optica Publishing Group, Washington, DC United States, 2020) pp. 1–2.
[44] H. Milchberg, Indestructible plasma optics, Phys. Today **72**, 70 (2019).
[45] C. G. Durfee and H. M. Milchberg, Light Pipe for High Intensity Laser Pulses, Phys. Rev. Lett. **71**, 2409 (1993).
[46] V. M. Malkin, G. Shvets, and N. J. Fisch, Fast Compression of Laser Beams to Highly Overcritical Powers, Phys. Rev. Lett. **82**, 4448 (1999).
[47] C. Thaury, F. Quéré, J. P. Geindre, A. Levy, T. Ceccotti, P. Monot, M. Bougeard, F. Réau, P. d'Oliveira, P. Audebert *et al.*, Plasma mirrors for ultrahigh-intensity optics, Nat. Phys. **3**, 424 (2007).
[48] G. Doumy, F. Quéré, O. Gobert, M. Perdrix, P. Martin, P. Audebert, J. C. Gauthier, J.-P. Geindre, and T. Wittmann, Complete characterization of a plasma mirror for the production of high-contrast ultraintense laser pulses, Phys. Rev. E **69**, 026402 (2004).
[49] B. Dromey, S. Kar, M. Zepf, and P. Foster, The plasma mirror—A subpicosecond optical switch for ultrahigh power lasers, Rev. Sci. Instrum. **75**, 645 (2004).
[50] H. C. Kapteyn, M. M. Murnane, A. Szoke, and R. W. Falcone, Prepulse energy suppression for high-energy ultrashort pulses using self-induced plasma shuttering, Opt. Lett. **16**, 490 (1991).
[51] P. Michel, L. Divol, E. A. Williams, S. Weber, C. A. Thomas, D. A. Callahan, S. W. Haan, J. D. Salmonson, S. Dixit, D. E. Hinkel, M. J. Edwards, B. J. MacGowan, J. D. Lindl, S. H. Glenzer, and L. J. Suter, Tuning the Implosion Symmetry of ICF Targets via Controlled Crossed-Beam Energy Transfer, Phys. Rev. Lett. **102**, 025004 (2009).
[52] P. Michel, L. Divol, E. A. Williams, C. A. Thomas, D. A. Callahan, S. Weber, S. W. Haan, J. D. Salmonson, N. B. Meezan, O. L. Landen, *et al.*, Energy transfer between laser beams crossing in ignition hohlraums, Phys. Plasmas **16**, 042702 (2009).
[53] G. Lehmann and K. H. Spatschek, Transient Plasma Photonic Crystals for High-Power Lasers, Phys. Rev. Lett. **116**, 225002 (2016).
[54] G. Lehmann and K. H. Spatschek, Laser-driven plasma photonic crystals for high-power lasers, Phys. Plasmas **24**, 056701 (2017).
[55] G. Lehmann and K. H. Spatschek, Plasma-based polarizer and waveplate at large laser intensity, Phys. Rev. E **97**, 063201 (2018).
[56] P. Michel, L. Divol, D. Turnbull, and J. D. Moody, Dynamic Control of the Polarization of Intense Laser Beams Via Optical Wave Mixing in Plasmas, Phys. Rev. Lett. **113**, 205001 (2014).
[57] P. Michel, E. Kur, M. Lazarow, T. Chapman, L. Divol, and J. S. Wurtele, Polarization-Dependent Theory of Two-Wave Mixing in Nonlinear Media, and Application to Dynamical Polarization Control, Phys. Rev. X **10**, 021039 (2020).
[58] E. Kur, M. Lazarow, J. S. Wurtele, and P. Michel, Nonlinear polarization transfer and control of two laser beams overlapping in a uniform nonlinear medium, Opt. Express **29**, 1162 (2021).
[59] L. Friedland and A. G. Shagalov, Standing autoresonant plasma waves, J. Plasma Phys. **86**, 825860301 (2020).
[60] L. Friedland, G. Marcus, J. S. Wurtele, and P. Michel, Excitation and control of large amplitude standing ion acoustic waves, Phys. Plasmas **26**, 092109 (2019).
[61] A. Scott, *Nonlinear Science: Emergence and Dynamics of Coherent Structures* (Oxford University Press, Oxford, 1999).
[62] S. Novikov, S. V. Manakov, L. P. Pitaevskii, and V. E. Zakharov, *Theory of Solitons: The Inverse Scattering Method* (Consultants Bureau, New York, 1984).
[63] L. Friedland and A. G. Shagalov, Emergence and Control of Multiphase Nonlinear Waves by Synchronization, Phys. Rev. Lett. **90**, 074101 (2003).

[64] L. Friedland and A. G. Shagalov, Excitation of multiphase waves of the nonlinear Schrödinger equation by capture into resonances, Phys. Rev. E **71**, 036206 (2005).
[65] A. Shagalov and L. Friedland, Autoresonant excitation of multiphase waves in the sine-Gordon model, Physica D **238**, 1561 (2009).
[66] M. Khasin and L. Friedland, Multiphase control of a nonlinear lattice, Phys. Rev. E **68**, 066214 (2003).
[67] L. Friedland and A. G. Shagalov, Excitation and control of chirped nonlinear ion-acoustic waves, Phys. Rev. E **89**, 053103 (2014).
[68] L. Friedland and A. G. Shagalov, Extreme driven ion acoustic waves, Phys. Plasmas **24**, 082106 (2017).
[69] H. Washimi and T. Taniuti, Propagation of Ion-Acoustic Solitary Waves of Small Amplitude, Phys. Rev. Lett. **17**, 996 (1966).
[70] G. B. Whitham, *Linear and Nonlinear Waves* (Wiley, New York, 1999).
[71] B. Kakad, A. Kakad, and Y. Omura, Particle trapping and ponderomotive processes during breaking of ion acoustic waves in plasmas, Phys. Plasmas **24**, 102122 (2017).
[72] C. Riconda, A. Heron, D. Pesme, S. Hüller, V. T. Tikhonchuk, and F. Detering, Electron Kinetic Effects in the Nonlinear Evolution of a Driven Ion-Acoustic Wave, Phys. Rev. Lett. **94**, 055003 (2005).
[73] I. Barth and L. Friedland, Multiresonant control of two-dimensional dynamical systems, Phys. Rev. E **76**, 016211 (2007).
[74] J. Fajans and L. Frièdland, Autoresonant (nonstationary) excitation of pendulums, plutinos, plasmas, and other nonlinear oscillators, Am. J. Phys. **69**, 1096 (2001).
[75] See Supplemental Material at http://link.aps.org/supplemental/10.1103/PhysRevResearch.4.023150 for an animation showing the crystallization of a single phase structure into a two-phase structure around the threshold.
[76] F. Wilczek, Quantum Time Crystals, Phys. Rev. Lett. **109**, 160401 (2012).
[77] A. Shapere and F. Wilczek, Classical Time Crystals, Phys. Rev. Lett. **109**, 160402 (2012).
[78] N. Y. Yao, C. Nayak, L. Balents, and M. P. Zaletel, Classical discrete time crystals, Nat. Phys. **16**, 438 (2020).
[79] D. V. Else, C. Monroe, C. Nayak, and N. Y. Yao, Discrete time crystals, Annu. Rev. Condens. Matter Phys. **11**, 467 (2020).
[80] N. Rao, P. Shukla, and M. Yu, Dust-acoustic waves in dusty plasmas, Planet. Space Sci. **38**, 543 (1990).